Hyperbolicity of general relativity in Bondi-like gauges

Thanasis Giannakopoulos, David Hilditch, and Miguel Zilhão
Centro de Astrofísica e Gravitação–CENTRA, Departamento de Física, Instituto Superior Técnico–IST, Universidade de Lisboa–UL, Avenida Rovisco Pais 1, 1049-001 Lisboa, Portugal

(Received 21 July 2020; accepted 17 August 2020; published 14 September 2020)

Bondi-like (single-null) characteristic formulations of general relativity are used for numerical work in both asymptotically flat and anti–de Sitter spacetimes. The well posedness of the resulting systems of partial differential equations, however, remains an open question. The answer to this question affects accuracy and, potentially, the reliability of conclusions drawn from numerical studies based on such formulations. A numerical approximation can converge to the continuum limit only for well-posed systems; for the initial value problem in the L^2 norm, this is characterized by strong hyperbolicity. We find that, due to a shared pathological structure, the systems arising from the aforementioned formulations are, however, only weakly hyperbolic. We present numerical tests for toy models that demonstrate the consequence of this shortcoming in practice for the characteristic initial boundary value problem. Working with alternative norms in which our model problems may be well posed, we show that convergence may be recovered. Finally, we examine the well posedness of a model for Cauchy-characteristic matching in which model symmetric and weakly hyperbolic systems communicate through an interface, with the latter playing the role of general relativity in the Bondi gauge on characteristic slices. We find that, due to the incompatibility of the norms associated with the two systems, the composite problem does not naturally admit energy estimates.

DOI: 10.1103/PhysRevD.102.064035

I. INTRODUCTION

Characteristic formulations of general relativity (GR) have advantages over more standard spacelike foliations in a number of situations. For instance, in the asymptotically flat setting, the Bondi-Sachs formalism [1,2], crucial to the modern understanding of gravitational waves, underpins codes that aim to produce waveforms of high accuracy. This approach exploits the fact that null hypersurfaces reach future null infinity and, hence, allows the avoidance of systematic errors from extrapolation techniques. The general setup in these approaches is to construct a standard Cauchy problem in a finite region of the spacetime, where the main action, such as the collision of two black holes, takes place. The data on the worldtube of this finite region serve as boundary data for the characteristic initial boundary value problem (CIBVP). Solving this CIBVP, one can compute quantities such as the gravitational wave news function at future null infinity. This method is often called *Cauchy-characteristic extraction* (CCE) [3–8]. If the Cauchy and the CIBVP are solved simultaneously and one attempts to match the worldtube data from both the Cauchy problem and the CIBVP, then the method is called *Cauchy-characteristic matching* (CCM); see [9,10] for a thorough review. In Fig. 1, an illustration of the geometric setup is given. Concerning asymptotically anti–de Sitter (AdS) spacetimes, characteristic formulations of GR are widely used in the field of numerical holography, which provides insights into the behavior of strongly coupled matter [11,12]. We refer to the aforementioned characteristic formulations as *Bondi-like* or *single null*.

A practical advantage of Bondi-like gauges is that the field equations can then be written as a set of nested differential equations which can be efficiently solved. For the resulting CIBVP, one provides data on a timelike boundary and initial data on either an outgoing or ingoing null hypersurface depending on the physical setup. There are many examples of numerical codes making successful use of this formalism. Since these codes have successfully passed a multitude of convergence tests, and in various physical contexts, one might say that there is numerical evidence that the partial differential equation (PDE) problem solved is well posed. To the best of our knowledge, however, a proof of this result is missing. By well posedness, we mean the usual notion that the problem admits unique solutions that depend continuously on the given data in a suitable norm. Interest in this property is not purely mathematical, since a numerical solution can converge to the continuous one only for well-posed PDE problems. The PDE systems that interest us here are of the hyperbolic class. A necessary condition for well posedness of these systems in L^2, or, in fact, suitable Sobolev norms, is that they are strongly hyperbolic [13,14]. Specifically, we consider PDEs in the generic form

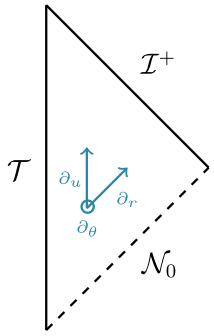

FIG. 1. The CIBVP for the wave zone of an asymptotically flat spacetime. Boundary data are given on the timelike inner boundary $\mathcal{T}$, the worldtube $r = r_0$, and initial data on the null hypersurface $\mathcal{N}_0$ of constant retarded time u_0.

$$\mathcal{A}^t(\mathbf{u}, x^\mu)\partial_t \mathbf{u} + \mathcal{A}^p(\mathbf{u}, x^\mu)\partial_p \mathbf{u} + \mathcal{S}(\mathbf{u}, x^\mu) = 0, \quad (1)$$

where $\mathbf{u} = (u_1, u_2, \ldots, u_q)^T$ is the state vector of the system and

$$\mathcal{A}^\mu = \begin{pmatrix} a^\mu_{11} & \cdots & a^\mu_{1q} \\ \vdots & \ddots & \vdots \\ a^\mu_{q1} & \cdots & a^\mu_{qq} \end{pmatrix}$$

denotes the principal part matrices, with $\det(\mathcal{A}^t) \neq 0$. To classify locally the character of the PDE, we linearize about a background solution and then work pointwise in the frozen coefficient approximation, henceforth suppressing the explicit dependencies of the principal part matrices and source vector and requesting the following definitions everywhere. We can construct the principal symbol

$$\mathbf{P}^s = (\mathcal{A}^t)^{-1}\mathcal{A}^p s_p, \quad (2)$$

where s^i is an arbitrary unit spatial vector. If $\mathbf{P}^s$ has real eigenvalues for all s^i, then the PDE system is called *weakly hyperbolic* (WH), whereas if, in addition, $\mathbf{P}^s$ is diagonalizable for all s^i, and there exists a constant K independent of s^i such that

$$|\mathbf{T}_s| + |\mathbf{T}_s^{-1}| \leq K,$$

with $\mathbf{T}_s$ the similarity matrix that diagonalizes $\mathbf{P}^s$, it is called *strongly hyperbolic* (SH).

Presently, we analyze the character of the PDE systems that arise in two specific Bondi-like formulations of GR. The original systems involve second-order derivatives, so we perform reductions to first order to conveniently build the principal parts. We find that, due to a degeneracy in the angular or transverse principal parts, these formulations are only WH. Consequently, they give rise to PDE problems that are ill posed in L^2 even in the linear, frozen coefficient approximation, which prohibits well posedness of the full system in associated Sobolev norms. We argue, furthermore, that this result holds true for every possible first-order reduction.

Subsequently, we perform careful numerical experiments that demonstrate the consequence of this shortcoming in practice. We work with two toy models, one of which is SH and the other only WH. We perform robust-stability-like [15,16] tests, suitably modified for the characteristic setting, and find that convergence in a discrete approximation to L^2 is prohibited in the WH model. Convergence with the latter model can be achieved by using a discrete approximation to a modified norm that involves a subset of derivatives of the state vector fields and adjusting the initial data for the test.

The structure of the paper is as follows. In Sec. II, we give an overview of popular Bondi-like formulations of GR in both the asymptotically flat and AdS contexts and present our hyperbolicity analysis of each. Afterward, in Sec. III, we present our toy models, and then in Sec. IV we present numerical experiments demonstrating the effect of our analytic results in practice. Finally, we conclude in Sec. V. Geometric units are used throughout.

II. CHARACTERISTIC FORMULATIONS

In this section, we present two characteristic formulations of GR in Bondi-like gauges that are widely used in numerical work. The first, the Bondi-Sachs formulation proper, is popular in the asymptotically flat setting, whereas the second, known as the affine-null system, is used most often in numerical holography. We demonstrate that each is only weakly hyperbolic.

A. Bondi-Sachs gauge

In the Bondi-Sachs gauge [1,2] a generic four-dimensional axially symmetric metric can be written as

$$ds^2 = \left(\frac{V}{r}e^{2\beta} - U^2 r^2 e^{2\gamma}\right)du^2 + 2e^{2\beta}dudr + 2Ur^2 e^{2\gamma}dud\theta - r^2(e^{2\gamma}d\theta^2 + e^{-2\gamma}\sin^2\theta d\phi^2). \quad (3)$$

Here u is a null coordinate, called retarded time, r is the areal radius, and θ, ϕ give coordinates on the two-sphere in the standard way. All metric functions are functions of (u, r, θ). To make contact with Ref. [9], we adopt the signature convention $(+, -, -, -)$. In this formulation, Einstein's equations exhibit a nested structure. For axially symmetric spacetimes, the PDE system consists of three equations intrinsic to the hypersurfaces of constant time:

$$
\begin{aligned}
\beta_{,r} &= \frac{1}{2} r(\gamma_{,r})^2, \\
[r^4 e^{2(\gamma-\beta)} U_{,r}]_{,r} &= 2r^2 \left[r^2 \left(\frac{\beta}{r^2} \right)_{,r\theta} - \frac{(\sin^2\theta\gamma)_{,r\theta}}{\sin^2\theta} + 2\gamma_{,r}\gamma_{,\theta} \right], \\
V_{,r} &= -\frac{1}{4} r^4 e^{2(\gamma-\beta)} (U_{,r})^2 + \frac{(r^4 \sin\theta U)_{,r\theta}}{2r^2 \sin\theta} \\
&\quad + e^{2(\beta-\gamma)} \left[1 - \frac{(\sin\theta\beta_{,\theta})_{,\theta}}{\sin\theta} + \gamma_{,\theta\theta} \right. \\
&\quad \left. + 3\cot\theta\gamma_{,\theta} - (\beta_{,\theta})^2 - 2\gamma_{,\theta}(\gamma_{,\theta} - \beta_{,\theta}) \right],
\end{aligned} \tag{4}
$$

and one equation that involves extrinsic derivatives:

$$
\begin{aligned}
4r(r\gamma)_{,ur} &= \left\{ 2r\gamma_{,r} V - r^2 \left[2\gamma_{,\theta} U + \sin\theta \left(\frac{U}{\sin\theta} \right)_{,\theta} \right] \right\}_{,r} \\
&\quad - 2r^2 \frac{(\gamma_{,r} U \sin\theta)_{,\theta}}{\sin\theta} + \frac{1}{2} r^4 e^{2(\gamma-\beta)} (U_{,r})^2 \\
&\quad + 2e^{2(\beta-\gamma)} \left[(\beta_{,\theta})^2 + \sin\theta \left(\frac{\beta_{,\theta}}{\sin\theta} \right)_{,\theta} \right].
\end{aligned} \tag{5}
$$

The remaining Einstein equations are not solved explicitly and, as in any other free-evolution approach, are therefore ignored in our analysis.

1. First-order reduction and linearization

In Refs. [17,18], the authors studied the existence and uniqueness of the CIBVP for the formulation given in the previous subsection. They considered the linearized and quasilinear systems but did not study continuous dependence on given data, which will be our main focus. To treat the system in the original higher-order derivative form, we could follow Refs. [19,20]. But for convenience in building the principal parts, we instead perform an explicit first-order reduction. Since this PDE is built as a reduction, there is the subtlety of the associated constraints and the specific choice of reduction, which we discuss in detail later. The minimal set of reduction variables are given by

$$
U_r = \partial_r U, \qquad \gamma_r = \partial_r \gamma, \qquad \gamma_\theta = \partial_\theta \gamma, \qquad \beta_\theta = \partial_\theta \beta.
$$

We linearize the resulting equations about a fixed background. In Ref. [21], one can find the complete analysis for both Minkowski and arbitrary backgrounds. The resulting level of hyperbolicity of the system is the same regardless, and so we present the former for brevity. After this procedure, the system reads

$$
\begin{aligned}
\partial_r \beta &= 0, \\
\partial_r U_r - \frac{2}{r^2} \partial_r \beta_\theta + \frac{2}{r^2} \partial_r \gamma_\theta + S_2 &= 0, \\
\partial_r V + \partial_\theta \beta_\theta - \partial_\theta \gamma_\theta - 2r\partial_\theta U - \frac{r^2}{2} \partial_\theta U_r + S_3 &= 0, \\
4r^2 \partial_u \gamma_r + 4r\partial_u \gamma - 2r^2 \partial_r \gamma_r + 2r\partial_\theta U & \\
+ r^2 \partial_\theta U_r - 2\partial_\theta \beta_\theta + S_4 &= 0, \\
\partial_r U + S_5 &= 0, \\
\partial_r \gamma + S_6 &= 0, \\
\partial_r \gamma_\theta - \partial_\theta \gamma_r &= 0, \\
\partial_r \beta_\theta &= 0,
\end{aligned} \tag{6}
$$

where S_i denotes the various source terms and we work in the frozen coefficient approximation, so that r and so forth must be treated as constants. The variables can be collected in the state vector

$$
\mathbf{u} = (\beta, \gamma, U, V, \gamma_r, U_r, \beta_\theta, \gamma_\theta)^T,
$$

and the system can be written in the form (1) with

$$
\boldsymbol{\mathcal{A}}^u \partial_u \mathbf{u} + \boldsymbol{\mathcal{A}}^r \partial_r \mathbf{u} + \boldsymbol{\mathcal{A}}^\theta \partial_\theta \mathbf{u} + \boldsymbol{\mathcal{S}} = 0. \tag{7}
$$

The principal part matrix $\boldsymbol{\mathcal{A}}^u$ associated with retarded time u is not invertible (see [21] for the full calculation). In order to use the standard definitions given in the introduction, we need a principal part associated to time derivatives that is invertible. We achieve this by performing a coordinate transformation to a frame that involves one timelike and three spacelike directions.

2. Coordinate transformation

We wish to bring the system (7) to the form (1), which has a trivial time principal part matrix

$$
\partial_t \mathbf{u} + \boldsymbol{\mathcal{A}}^p \partial_p \mathbf{u} + \boldsymbol{\mathcal{S}} = 0,
$$

where ∂_p denotes spatial derivatives and $\mathbf{u}$ denotes the state vector. We therefore perform the following concrete coordinate transformation:

$$
u = t - \rho, \quad r = \rho, \tag{8}
$$

with the angular coordinates unchanged, which yields the following relation between the old and new basis vectors:

$$
\partial_u = \partial_t, \qquad \partial_r = \partial_t + \partial_\rho,
$$

with the remaining vectors unaltered. A schematic of the auxiliary setup is given in Fig. 2. Applying the transformation yields

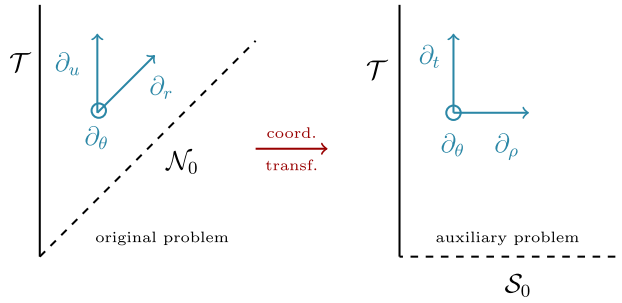

FIG. 2. The original CIBVP is transformed into an auxiliary frame using the coordinate transformation (8) as shown. This allows the use of textbook definitions of hyperbolicity but does not affect the solution space.

$$\boldsymbol{\mathcal{A}}^t\partial_t\mathbf{u} + \boldsymbol{\mathcal{A}}^r\partial_\rho\mathbf{u} + \boldsymbol{\mathcal{A}}^\theta\partial_\theta\mathbf{u} + \boldsymbol{\mathcal{S}} = 0,$$

with $\boldsymbol{\mathcal{A}}^t = \boldsymbol{\mathcal{A}}^u + \boldsymbol{\mathcal{A}}^r$ invertible. After multiplying on the left with the inverse of $\boldsymbol{\mathcal{A}}^t$, we bring the system to the desired form:

$$\partial_t\mathbf{u} + \mathbf{B}^\rho\partial_\rho\mathbf{u} + \mathbf{B}^{\hat{\theta}}\partial_{\hat{\theta}}\mathbf{u} + \mathbf{S} = 0, \tag{9}$$

where $\mathbf{B}^\rho = (\boldsymbol{\mathcal{A}}^t)^{-1}\boldsymbol{\mathcal{A}}^r$ and $\mathbf{B}^{\hat{\theta}} = \rho(\boldsymbol{\mathcal{A}}^t)^{-1}\boldsymbol{\mathcal{A}}^\theta$ with $\partial_{\hat{\theta}} \equiv 1/\rho\partial_\theta$ and $\mathbf{S}$ was redefined in the obvious manner. The solution space in this frame is equivalent to that of the original one, so in this sense the character of the PDE is invariant. For our system, the principal part matrix $\mathbf{B}^\rho$ is diagonalizable with real eigenvalues. Although $\mathbf{B}^{\hat{\theta}}$ has real eigenvalues, it does not have a complete set of eigenvectors and, hence, is not diagonalizable. Therefore, the system resulting from the specific first-order reduction we made is only WH. In Ref. [22], a subsystem of a similar first-order reduction was shown to be symmetric hyperbolic. Here, however, we are concerned with the best estimates that can be made for the full system. In Sec. III, this is written up explicitly for our homogeneous WH model.

So far, we have not ruled out the existence of an alternative first-order reduction that *is* SH, however. To examine this possibility, we have to understand if any potential addition of reduction constraints can make the system SH. The reduction constraints are

$$\partial_\theta\beta - \beta_\theta = 0, \qquad \partial_\theta\gamma - \gamma_\theta = 0. \tag{10}$$

The definitions of the variables γ_r and U_r are solved explicitly as time evolution equations within the system (6) and, therefore, do not have an associated constraint. This subtlety, along with an examination of the form of the degeneracy, follows in the next section.

3. Generalized characteristic variables

To understand the nature of the degeneracy of $\mathbf{B}^{\hat{\theta}}$ physically, it is useful to consider the generalized eigenvalue problem

$$\mathbf{l}_{\lambda_i}(\mathbf{B}^{\hat{\theta}} - \lambda_i\mathbb{1})^m = 0,$$

with λ_i standing for the various eigenvalues and $\mathbf{l}_{\lambda_i}$ representing either a true eigenvector when $m = 1$ or else a generalized eigenvector when $m > 1$. The eigenvalues of $\mathbf{B}^{\hat{\theta}}$ are $\lambda = \pm 1$, each with algebraic multiplicity one, and $\lambda = 0$ with algebraic multiplicity six. The geometric multiplicity of each of $\lambda = \pm 1$ is also one, but $\lambda = 0$ has geometric multiplicity five. In other words, one associated eigenvector is missing, and we obtain one nontrivial generalized eigenvector with $m = 2$ for $\lambda = 0$. Defining the invertible matrix $\mathbf{T}^{-1}_{\hat{\theta}}$ with the vectors $\mathbf{l}_{\lambda_i}$, as rows, we obtain the Jordan normal form of the principal symbol in the θ direction by the similarity transformation

$$\mathbf{J}^{\hat{\theta}} \equiv \mathbf{T}^{-1}_{\hat{\theta}}\mathbf{B}^{\hat{\theta}}\mathbf{T}_{\hat{\theta}}.$$

The same matrix can be used to construct the generalized characteristic variables of the system in the θ direction, namely, the components of $\mathbf{v} \equiv \mathbf{T}^{-1}_{\hat{\theta}}\mathbf{u}$. These are, of course, nothing more than the left generalized eigenvectors contracted with the state vector. Working as before in the frozen coefficient approximation, focusing on the t, θ parts of (9), and multiplying on the left with $\mathbf{T}^{-1}_{\hat{\theta}}$, we get

$$\partial_t\mathbf{v} + \mathbf{J}_{\hat{\theta}}\partial_{\hat{\theta}}\mathbf{v} \simeq 0, \tag{11}$$

with $\simeq$ denoting here equality up to nonprincipal terms and spatial derivatives transverse to $\partial_{\hat{\theta}}$. The generalized characteristic variables with speed (eigenvalue) zero are

$$\rho U + \frac{\rho^2}{2}U_r - \beta_\theta + \gamma_\theta, \qquad \beta_\theta, \qquad V,$$
$$\rho\left(-2\rho U - \frac{\rho^2}{2}U_r + \beta_\theta - \gamma_\theta\right), \qquad \gamma, \qquad \beta,$$

of which the third and fourth are associated with the nontrivial 2×2 Jordan block within $\mathbf{J}^{\hat{\theta}}$. Likewise, we have

$$-\frac{\rho}{2}U + \frac{\rho}{2}\gamma_r - \frac{\rho^2}{4}U_r + \frac{1}{2}\beta_\theta,$$
$$-\frac{\rho}{2}U - \frac{\rho}{2}\gamma_r - \frac{\rho^2}{4}U_r + \frac{1}{2}\beta_\theta,$$

with speeds ± 1, respectively. The structure of $\mathbf{J}_{\hat{\theta}}$ thus yields

$$-\partial_t\left(2\rho U + \frac{\rho^2}{2}U_r - \beta_\theta + \gamma_\theta\right) \simeq 0,$$
$$\partial_t V - \rho\partial_{\hat{\theta}}\left(2\rho U + \frac{\rho^2}{2}U_r - \beta_\theta + \gamma_\theta\right) \simeq 0. \tag{12}$$

Strongly hyperbolic systems admit a complete set of characteristic variables in each direction. In other words, if our system were strongly hyperbolic, then up to non-principal and transverse derivative terms each component of $\mathbf{v}$ would satisfy an advection equation. Presently, the best we can achieve for V, however, is (12). Physically, we may therefore understand weak hyperbolicity as the failure of V, a *generalized* characteristic variable, to satisfy such an advection equation. As mentioned in the previous section, we could try to cure the equations by using a different first-order reduction. Observe that the choice of different reductions corresponds to the freedom to add (derivatives of) the reduction constraints to (12) without introducing second derivatives. As V appears at most once differentiated in the original equations, there is no associated constraint, so we must hope to eradicate the ∂_θ term from (12) using (10) without introducing second derivatives. Even if the variable $U_\theta = \partial_\theta U$ were introduced in the reduction, however, the $\partial_\theta\beta_\theta$ and $\partial_\theta\gamma_\theta$ terms would obviously persist. Thus, one nontrivial *generalized* characteristic variable always survives and prevents the existence of a complete set of characteristic variables. Hence, within the coordinate basis built from (t,ρ,θ), the field equations are at best only weakly hyperbolic regardless of the specific reduction.

B. Affine-null gauge

Although sometimes used in the asymptotically flat setting [23,24], the affine-null gauge is particularly popular for evolutions in asymptotically AdS spacetimes [25]. For concreteness, we will treat the specific system that occurs in the case of asymptotically AdS_5 spaces with planar symmetry, but we expect similar results in other contexts with analogous gauges. The metric is written as

$$ds^2 = -Adv^2 + \Sigma^2[e^B dx_\perp^2 + e^{-2B}dz^2] + 2dRdv + 2Fdvdz. \tag{13}$$

Here v denotes a null coordinate, called advanced time, and R is called the holographic coordinate and increases from the bulk of the spacetime toward the boundary. All metric components are functions of (v,R,z). We also denote by $dx_\perp^2$ the flat metric in the plane spanned by $x_\perp$, the two coordinates associated with the symmetry. Using the convenient definitions

$$d_z \equiv \partial_z - F\partial_R, \qquad d_+ \equiv \partial_v + \frac{A}{2}\partial_R, \tag{14}$$

the field equations can be succinctly stated and are

$$\begin{aligned}
\partial_R^2\Sigma &= -\frac{1}{2}(\partial_R B)^2\Sigma,\\
\Sigma^2\partial_R^2 F &= \Sigma(6d_z\Sigma\partial_R B + 4\partial_R d_z\Sigma + 3\partial_R F\partial_R\Sigma) + \Sigma^2(3d_z B\partial_R B + 2\partial_R d_z B) - 4d_z\Sigma\partial_R\Sigma,\\
12\Sigma^3\partial_R d_+\Sigma &= -8\Sigma^2(-3\Sigma^2 + 3d_+\Sigma\partial_R\Sigma) + e^{2B}\{\Sigma^2[4d_z B\partial_R F - 4d_z^2 B - 7(d_z B)^2 + 2\partial_R d_z F + (\partial_R F)^2] + 4(d_z\Sigma)^2\\
&\quad + 2\Sigma[d_z\Sigma(\partial_R F - 8d_z B) - 4d_z^2\Sigma]\},\\
6\Sigma^4\partial_R d_+ B &= -9\Sigma^3(\partial_R\Sigma d_+ B + \partial_R B d_+\Sigma) + e^{2B}\{\Sigma^2[(d_z B)^2 - d_z B\partial_R F + d_z^2 B - 2\partial_R d_z F - (\partial_R F)^2] - 4(d_z\Sigma)^2\\
&\quad + \Sigma[d_z\Sigma(d_z B + 4\partial_R F) + 2d_z^2\Sigma]\},\\
6\Sigma^4\partial_R^2 A &= 72\Sigma^2 d_+\Sigma\partial_R\Sigma - 2\Sigma^4(9\partial_R B d_+ B + 12) + 3e^{2B}\{\Sigma^2[4d_z^2 B + 7(d_z B)^2 - (\partial_R F)^2]\\
&\quad + 8\Sigma(2d_z B d_z\Sigma + d_z^2\Sigma) - 4(d_z\Sigma)^2\},
\end{aligned} \tag{15}$$

and, finally,

$$\partial_v B = d_+ B - \frac{A}{2}\partial_R B. \tag{16}$$

As in the previous section, there are also two additional equations that are not explicitly solved. The vector d_+ points to the direction of the outgoing null rays, and, hence, Eqs. (15) do involve derivatives extrinsic to the hypersurfaces of constant time. However, if one considers d_+B and $d_+\Sigma$ as independent variables of the system, then Eqs. (15) are intrinsic to the ingoing null hypersurfaces and possess a nested structure just as in the Bondi gauge. Hence, the only equation that involves derivatives extrinsic to the hypersurfaces of constant retarded time is (16). To analyze the hyperbolicity of the resulting PDE system, we follow exactly the same steps as in the previous setup.

1. First-order reduction and linearization

The definition (14) was used earlier to write the field equations in a more compact form, but for the rest of the analysis we expand out the definition of d_z. Before performing the first-order reduction, we apply the coordinate transformation $r = 1/R$, drawing the boundary to $r = 0$. The metric components, however, still exhibit singular behavior there, so, as elsewhere in the literature,

we apply appropriate field redefinitions to obtain regular fields on the boundary, namely,

$$A(v,r,z) \to \frac{1}{r^2} + r^2 A(v,r,z),$$
$$B(v,r,z) \to r^4 B(v,r,z),$$
$$\Sigma(v,r,z) \to \frac{1}{r} + r^3 \Sigma(v,r,z),$$
$$F(v,r,z) \to r^2 F(v,r,z),$$

and similarly for derivatives of the above fields. To simplify the presentation, we linearize here about vacuum AdS. Our conclusions are, however, unaltered if we work about an arbitrary background. Full expressions in the general case can be found in Ref. [21]. We define reduction variables according to

$$A_r = \partial_r A, \quad B_r = \partial_r B, \quad F_r = \partial_r F, \quad \Sigma_r = \partial_r \Sigma,$$
$$A_z = \partial_z A, \quad B_z = \partial_z B, \quad F_z = \partial_z F, \quad \Sigma_z = \partial_z \Sigma,$$
$$B_+ = d_+ B, \quad \Sigma_+ = d_+ \Sigma.$$

The complete first-order system is then

$$\begin{aligned}
r^4 \partial_v B &= -S_1,\\
r^4 \partial_v B_r &= \frac{r^4}{2}\partial_r B_r + r^3 \partial_r B_+ - S_2,\\
-6r\partial_r B_+ &= 2r^2 \partial_r F_z + r^2 \partial_z B_z + 2r^2 \partial_z \Sigma_z - S_3,\\
\partial_r B_z &= \partial_z B_r,\\
\partial_r \Sigma &= -S_5,\\
r^7 \partial_r \Sigma_r &= -S_6,\\
12r\partial_r \Sigma_+ &= 2r^2 \partial_r F_z + 4r^2 \partial_z B_z + 8r^2 \partial_z \Sigma_z - S_7,\\
\partial_r \Sigma_z &= \partial_z \Sigma_r,\\
\partial_r F &= -S_9,\\
r^4 \partial_r F_r &= -4r^4 \partial_r \Sigma_z - 2r^4 \partial_r B_z - S_{10},\\
\partial_r F_z &= \partial_z F_r,\\
\partial_r A &= -S_{12},\\
6r^2 \partial_r A_r &= 12r^2 \partial_z B_z + 24 r^2 \partial_z \Sigma_z - S_{13},\\
\partial_r A_z &= \partial_z A_r,
\end{aligned} \tag{17}$$

which can be written as

$$\boldsymbol{\mathcal{A}}^v \partial_v \mathbf{u} + \boldsymbol{\mathcal{A}}^r \partial_r \mathbf{u} + \boldsymbol{\mathcal{A}}^z \partial_z \mathbf{u} + \boldsymbol{\mathcal{S}} = 0, \tag{18}$$

with state vector

$$\mathbf{u} = (A_r, B_+, \Sigma_+, \Sigma_r, F_r, B_z, \Sigma_z, B_r, A_z, F_z, A, F, B, \Sigma)^T.$$

The principal part matrix associated with the retarded advanced time $\boldsymbol{\mathcal{A}}^v$ is again not invertible, and, hence, we proceed with a transformation to an appropriate auxiliary frame.

2. Coordinate transformation

To obtain a suitable coordinate frame, we transform from (v,r,z) to (t,ρ,z) with

$$v = t - \rho, \quad r = \rho,$$

and the remaining coordinates unaltered, which gives

$$\partial_v = \partial_t, \qquad \partial_r = \partial_t + \partial_\rho,$$

with ∂_z unaffected. Applying the transformation yields

$$\boldsymbol{\mathcal{A}}^t \partial_t \mathbf{u} + \boldsymbol{\mathcal{A}}^r \partial_\rho \mathbf{u} + \boldsymbol{\mathcal{A}}^z \partial_z \mathbf{u} + \boldsymbol{\mathcal{S}} = 0,$$

where now $\boldsymbol{\mathcal{A}}^t = \boldsymbol{\mathcal{A}}^v + \boldsymbol{\mathcal{A}}^r$ is invertible. After multiplying from the left with the inverse of $\boldsymbol{\mathcal{A}}^t$, we again bring the system to the form

$$\partial_t \mathbf{u} + \mathbf{B}^\rho \partial_\rho \mathbf{u} + \mathbf{B}^z \partial_z \mathbf{u} + \mathbf{S} = 0, \tag{19}$$

where $\mathbf{B}^\rho = (\boldsymbol{\mathcal{A}}^t)^{-1}\boldsymbol{\mathcal{A}}^r$ and $\mathbf{B}^z = (\boldsymbol{\mathcal{A}}^t)^{-1}\boldsymbol{\mathcal{A}}^z$. The principal part $\mathbf{B}^\rho$ is diagonalizable with real eigenvalues 0 and ± 1. The principal part $\mathbf{B}^z$ has the same real eigenvalues, but it does not have a complete set of eigenvectors, so it is not diagonalizable. The system resulting from this specific first-order reduction is thus only WH. Next, by again constructing generalized characteristic variables in the z direction, we will examine whether or not an appropriate addition of the reduction constraints can render the reduction strongly hyperbolic. The reduction constraints are

$$\begin{aligned}
\partial_z A - A_z &= 0, \qquad \partial_z B - B_z = 0,\\
\partial_z \Sigma - \Sigma_z &= 0, \qquad \partial_z F - F_z = 0,\\
\partial_z B_\rho - \partial_\rho B_z &= \frac{1}{2}\partial_z B_r - \partial_z B_+ - \partial_\rho B_z = 0,\\
\partial_z \Sigma_\rho - \partial_\rho \Sigma_z &= \frac{1}{2}\partial_z \Sigma_r - \partial_z \Sigma_+ - \partial_\rho \Sigma_z = 0.
\end{aligned} \tag{20}$$

3. Generalized characteristic variables

The eigenvalues of $\mathbf{B}^z$ are $\lambda = \pm 1$ with algebraic multiplicity one and $\lambda = 0$ with algebraic multiplicity 12. There is one eigenvector for $\lambda = 1$, one for $\lambda = -1$, and nine for $\lambda = 0$. Since the algebraic and geometric multiplicity of $\lambda = 0$ differ by three, the Jordan normal form

$$\mathbf{J}^z \equiv \mathbf{T}_z^{-1} \mathbf{B}^z \mathbf{T}_z$$

must have some nontrivial block. Let us consider the t, z part of (19) and, as earlier in (11), use $\mathbf{T}_z^{-1}$ to construct the generalized characteristic variables in the z direction:

$$\mathbf{v} = \mathbf{T}_z^{-1}\mathbf{u} \tag{21}$$

satisfying

$$\partial_t \mathbf{v} + \mathbf{J}_z \partial_z \mathbf{v} \simeq 0, \tag{22}$$

with $\simeq$ here denoting equality up to transverse derivatives and nonprincipal terms. The components of $\mathbf{v}$ begin

$$-B_r - \frac{1}{3}B_z - \frac{2}{3}F_r - 2\Sigma_r - \frac{2}{3}\Sigma_z,$$
$$-B_r + \frac{1}{3}B_z + \frac{2}{3}F_r - 2\Sigma_r + \frac{2}{3}\Sigma_z,$$

with speeds ∓ 1, respectively. Next, we have those with vanishing speeds, which are most naturally presented in three blocks. The first of these consists of the set of *true* characteristic variables:

$$B_+ - \frac{\rho}{2}B_r - \rho\Sigma_r, \qquad \Sigma_+ - \frac{\rho}{8}A_r + \frac{\rho}{4}B_r + \frac{\rho}{2}\Sigma_r,$$
$$\frac{1}{4}A_r + \frac{3}{2}B_r + F_z + 3\Sigma_r, \qquad A, F, B, \Sigma,$$

a coupled pair consisting of one generalized and one characteristic variable, respectively,

$$-\frac{4}{3}B_z - \frac{2}{3}F_r - \frac{2}{3}\Sigma_z, \qquad -2\Sigma_r, \tag{23}$$

and finally a coupled triplet of two generalized characteristic variables and one characteristic variable, respectively,

$$\frac{1}{4}A_z + \frac{1}{6}B_z + \frac{1}{3}F_r + \frac{1}{3}\Sigma_z, \qquad -\frac{1}{4}A_r + \frac{1}{2}B_r + \Sigma_r,$$
$$\frac{2}{3}B_z + \frac{1}{3}F_r + \frac{4}{3}\Sigma_z. \tag{24}$$

In other words, from the structure of the Jordan blocks of $\mathbf{J}^z$, reading off the components of (22) the first member of the pair (23) and the first two members of the triple (24), we have the schematic form

$$\partial_t v_i + \partial_z v_{i+1} \simeq 0, \tag{25}$$

with v_i referring to the field and v_{i+1} the next element of the pair or triple. The question is whether or not there exists an appropriate addition of the reduction constraints (20) such that equations of the form (25) are turned into equations of the form

$$\partial_t v_i + \lambda_i \partial_z v_i \simeq 0, \tag{26}$$

where we are allowing different first-order reductions to adjust also characteristic speeds. This is a necessary condition for building an alternative reduction that is SH. This would mean that the generalized characteristic variable v_i that is originally coupled with v_{i+1} could be decoupled, and the respective generalized eigenvector replaced by a simple eigenvector. We examine this for the second two elements of the triplet (24) and show by contradiction that this necessary condition cannot be fulfilled. With our original, specific reduction, we have

$$\partial_t\left(\frac{2}{3}B_z + \frac{1}{3}F_r + \frac{4}{3}\Sigma_z\right) \simeq 0,$$
$$\partial_t\left(-\frac{1}{4}A_r + \frac{1}{2}B_r + \Sigma_r\right) + \partial_z\left(\frac{2}{3}B_z + \frac{1}{3}F_r + \frac{4}{3}\Sigma_z\right) \simeq 0. \tag{27}$$

Observe, first of all, that neither of these two equations, nor the two large terms grouped separately in the second, can be written as a linear combination (equality taken here in the sense of $\simeq$) of the reduction constraints (20). The choice of reduction lies in the freedom to add multiples of the six reduction constraints (20) to the evolution equations. Suppose that some choice of addition of these constraints did result in a SH first-order reduction. Starting with the first equation of (27), for our alternative reduction we have

$$\partial_t\left(\frac{2}{3}B_z + \frac{1}{3}F_r + \frac{4}{3}\Sigma_z\right) \simeq \sum_\alpha c_\alpha C_\alpha, \tag{28}$$

with the terms on the right-hand side a linear combination of the reduction constraints C_α. Since this alternative reduction is SH, we have

$$\sum_\alpha c_\alpha C_\alpha \simeq \sum_\alpha a_\alpha^0 \partial_z v_\alpha^0 + \sum_\alpha a_\alpha^\pm \partial_z v_\alpha^\pm,$$

with v_α^0 denoting the set of 0-speed characteristic variables and $v_\alpha^\pm$ denoting the remaining characteristic variables. Using $\partial_t v_\alpha^\pm \simeq \lambda_\alpha \partial_z v_\alpha^\pm$, we may therefore rewrite (28) as

$$\partial_t\left(\frac{2}{3}B_z + \frac{1}{3}F_r + \frac{4}{3}\Sigma_z - \sum_\alpha a_\alpha^\pm \lambda_\alpha^{-1} v_\alpha^\pm\right) \simeq \sum_\alpha a_\alpha^0 \partial_z v_\alpha^0.$$

Now, by our observation directly after (27), the term inside the large parentheses cannot vanish identically. Therefore, we must have $a_\alpha^0 = 0$, or we have found, on the left-hand side, a nontrivial generalized characteristic variable, in contradiction to the assumption that our reduction is SH. Moving on to the second equation of (27), we can write the equivalent expression for the alternative first-order reduction as

$$\partial_t\left(-\frac{1}{4}A_r+\frac{1}{2}B_r+\Sigma_r\right)+\partial_z\left(\frac{2}{3}B_z+\frac{1}{3}F_r+\frac{4}{3}\Sigma_z\right)\simeq\sum_\alpha c'_\alpha C_\alpha,$$

again with the right-hand side a linear combination of the reduction constraints. From here, a simple calculation shows that

$$-\frac{1}{4}A_r+\frac{1}{2}B_r+\Sigma_r+\sum_\alpha a'_\alpha\lambda_\alpha^{-1}v_\alpha^\pm$$

is nevertheless *still* a nontrivial generalized characteristic variable for a suitable choice of a'_α. By contradiction, we have therefore shown that there is no first-order reduction that gives a SH first-order PDE system in the (t,ρ,z) frame used here.

C. Frame independence

In the previous subsections, we presented a hyperbolicity analysis of two widely used Bondi-like formulations of GR. We worked with a particular auxiliary frame with one timelike element and the remainder spacelike. The auxiliary basis was used to express the original PDEs, which were then shown to be only WH. In this subsection, we argue that this result persists for other auxiliary frames. Our argument is based on the dual foliation (DF) approach of Ref. [26] and follows closely Sec. II.D of Ref. [27]. In this subsection, Latin letters $a\ldots e$ are used as abstract indices, Greek letters run from 0 to $d+1$ for a $d+1$-dimensional spacetime, and a given basis and Latin indices i,j,k denote only the spatial components of this basis. We also use p as an abstract index for the spatial derivatives appearing on the right-hand side of a first-order PDE. The symbol ∂_α stands for the flat covariant derivative naturally defined by x^μ.

The idea of the DF approach is to express a region of spacetime in terms of two different frames, which we call uppercase and lowercase. Considering a $d+1$ split of the spacetime, let us denote as n^a and N^a the normal vectors on the hypersurfaces of constant time for the lower- and uppercase frames, respectively. We call v^a and V^a the boost vectors for each frame, which are spatial with respect to the corresponding normal vector. The Lorentz factor is $W=(1-v^a v_a)^{-1/2}=(1-V^aV_a)^{-1/2}$, and we denote as γ_{ab} and ${}^{(N)}\gamma_{ab}$ the lower- and uppercase spatial metrics, respectively. The following useful relations hold:

$$\delta^a{}_b=\gamma^a{}_b-n^an_b={}^{(N)}\gamma^a{}_b-N^aN_b,\qquad n^a=W(N^a+V^a),\qquad N^a=W(n^a+v^a).\tag{29}$$

Let us consider a first-order PDE in the compact form

$$\mathcal{A}^b\delta^a{}_b\partial_a\mathbf{u}+\mathcal{S}=0,$$

and $d+1$ split using the lower- and uppercase frames, replacing $\delta^a{}_b$ by means of (29), giving

$$\mathcal{A}^n\partial_n\mathbf{u}\simeq\mathcal{A}^b\gamma^a{}_b\partial_a\mathbf{u},\quad \mathcal{A}^N\partial_N\mathbf{u}\simeq\mathcal{A}^{b(N)}\gamma^a{}_b\partial_a\mathbf{u}.\tag{30}$$

We obtain two evolution systems for the variables of $\mathbf{u}$, with

$$\mathcal{A}^an_a\equiv\mathcal{A}^n,\qquad n^a\partial_a\equiv\partial_n,\qquad \mathcal{A}^aN_a\equiv\mathcal{A}^N,\qquad N^a\partial_a\equiv\partial_N.\tag{31}$$

Without loss of generality, we choose to identify the uppercase frame with the auxiliary frames used in Secs. II A and II B. The definitions

$$\mathcal{A}^n\equiv\mathbf{A}^n,\qquad \mathcal{A}^a\gamma^b{}_a\equiv\mathbf{A}^b,\qquad \mathcal{A}^N\equiv\mathbf{B}^N,\qquad \mathcal{A}^{a(N)}\gamma^b{}_a\equiv\mathbf{B}^b,$$

imply $\mathbf{B}^bN_b=0$, $\mathbf{A}^bn_b=0$ and lead to the following upper- and lowercase first-order PDE forms, respectively:

$$\partial_N\mathbf{u}=\mathbf{B}^p\partial_p\mathbf{u}-\mathbf{S},\qquad \mathbf{A}^n\partial_n\mathbf{u}=\mathbf{A}^p\partial_p\mathbf{u}-\mathbf{S},\tag{32}$$

where $\mathbf{B}^N=\mathbb{1}$ by assumption. The former is the same form as in Eqs. (9) and (19). In this form, we found the PDE systems only WH due to the 2×2 Jordan blocks of the angular principal parts. This can be represented in a generalized eigenvalue problem of the form

$$\mathbf{l}^N_{\lambda_N}(\mathbf{P}^S-\mathbb{1}\lambda_N)^M=0,\tag{33}$$

where S^a is a unit spatial vector, $\mathbf{P}^S\equiv\mathbf{B}^aS_a$ is the principal symbol, and M is the rank of the generalized left eigenvector $\mathbf{l}^N_{\lambda_N}$ with eigenvalue λ_N, with $M=2$ for the generalized eigenvectors that correspond to the aforementioned Jordan blocks. We wish to examine if generalized eigenvalue problems of this form exist also in the lowercase frame. Hence, we need to relate the two equations of (32), obtaining

$$\mathbf{A}^n=W(\mathbb{1}+\mathbf{B}^V),\qquad \mathbf{A}^p=\mathbf{B}^a(\gamma^p{}_a+WV_av^p)-W(\mathbb{1}+\mathbf{B}^V)v^p,\tag{34}$$

and

$$\mathbf{B}^N=\mathbb{1}=W(\mathbf{A}^n+\mathbf{A}^v),\qquad \mathbf{B}^p=\mathbf{A}^{a(N)}\gamma^p{}_a-W\mathbf{A}^nV^p,\tag{35}$$

where we write $\mathbf{B}^aV_a\equiv\mathbf{B}^V$. Let us examine $\mathbb{1}+\mathbf{B}^V$. In Ref. [27], invertibility of this matrix was guaranteed by strong hyperbolicity. Here we want to analyze PDEs that are only WH and so may not assume that $\mathbf{B}^V$ is diagonalizable. Hence, let us denote as

$$\mathbf{J}^{S_V} = \mathbf{T}_{S_V}^{-1}\mathbf{B}^{S_V}\mathbf{T}_{S_V}$$

the Jordan normal form of $\mathbf{B}^{S_V} = \mathbf{B}^a(S_V)_a$, where $V^a = |V|S_V^a$ is the uppercase boost vector with norm $|V|$ pointing in the direction of S_V^a. One can write each block $\mathbf{j}$ of the Jordan form $\mathbf{J}$ with only the eigenvalue λ_i on the diagonal as

$$\mathbf{j} = \lambda_i \mathbb{1} + \mathbf{N},$$

where $\mathbf{N}$ is a nilpotent matrix of the size of $\mathbf{j}$ with $\mathbf{N}^q = 0$. Consequently,

$$\mathbf{T}_{S_V}^{-1}(\mathbb{1} + \mathbf{B}^V)\mathbf{T}_{S_V} = \mathbb{1} + \mathbf{J}^{S_V}|V|,$$

and for each block $\mathbf{j}^{S_V}$,

$$\mathbb{1} + \mathbf{j}^{S_V} = \tilde{\lambda}_i^{S_V}\left(\mathbb{1} + \frac{|V|}{\tilde{\lambda}_i^{S_V}}\mathbf{N}^{S_V}\right),$$

assuming that

$$\tilde{\lambda}_i^{S_V} = 1 + |V|\lambda_i^{S_V} \neq 0. \tag{36}$$

The inverse of this block is then

$$\frac{1}{\tilde{\lambda}_i^{S_V}}\left[\mathbb{1} + \sum_{j=1}^{q-1}\left(-\frac{|V|}{\tilde{\lambda}_i^{S_V}}\right)^j(\mathbf{N}^{S_V})^j\right],$$

and, hence, $\mathbb{1} + \mathbf{B}^V$ is invertible as long as condition (36) is satisfied for each λ_i. Note that in our normalization light speed corresponds to $\lambda = 1$. Since $|V| < 1$, inequality (36) is always satisfied for physical propagation speeds, although it could be violated when superluminal gauge speeds are present. If one considers, for instance, the analysis of Secs. II A and II B on top of Minkowski and vacuum AdS background, respectively, then this condition is satisfied. We wish to find the equivalent of the uppercase generalized eigenvalue problem (33) in the lowercase frame. Thus, using the second equation of (35) and $S_a = \mathbb{s}_a - WV^S n_a$ [27,28], we express the principal symbol in the lowercase frame, namely,

$$\mathbf{P}^S \equiv \mathbf{B}^a S_a = \mathbf{A}^a \mathbb{s}_a - \mathbf{A}^n W V^S.$$

Hence, the equivalent of (33) in the lowercase frame is

$$\mathbf{l}_{\lambda_N}^N[\mathbf{A}^{(\mathbb{s}-\lambda_N W v)} - W(\lambda_N + V^S)\mathbf{A}^n]^M = 0. \tag{37}$$

Thus, if in the uppercase frame the eigenproblem (33) with $M = 1$ fails to admit a complete set of left eigenvectors, then so does the lowercase frame, and so both setups would be at best weakly hyperbolic. To see this, we need only set $M = 1$ in (37) and note that the lowercase principal symbol in the $\mathbb{s}_a - \lambda_N W v_a$ direction is proportional to

$$(\mathbf{A}^n)^{-1}\mathbf{A}^{(\mathbb{s}-\lambda_N W v)},$$

and so deficiency of the lowercase principal symbol in this direction is equivalent to that of the uppercase principal symbol stated before. Unfortunately, the relationship between the upper- and lowercase generalized left eigenvectors is more subtle. Returning to our specific systems and identifying the uppercase unit spatial vector S^a with the unit spatial vectors in the ∂_θ and ∂_z directions of Sec. II, we conclude that weak hyperbolicity of those PDEs persists in other frames.

III. TOY MODELS

In this section, we introduce two toy models, one SH and one WH, which capture the core structure of the systems analyzed in the previous section. Our aim is to examine the consequence of the algebraic properties determined earlier on local well posedness in the context of the CIBVP. The principal parts of the two models differ only in the angular direction z, with the WH model possessing a nondiagonalizable principal symbol.

A. The PDEs

The equations of motion for the WH model are

$$\begin{aligned}\partial_x\phi &= -S_\phi,\\ \partial_x\psi_v - \partial_z\phi &= -S_{\psi_v},\\ \partial_u\psi - \frac{(1-x^2)^{3/2}}{2c_x}\partial_x\psi - \partial_z\psi &= -S_\psi,\end{aligned} \tag{38}$$

with $x \in [0,1]$, $z \in [0, 2\pi)$ with periodic boundary conditions, $u \geq u_0$ for some initial time u_0, and c_x a constant. This PDE can be written in the form

$$\mathbf{A}^u\partial_u\mathbf{u} + \mathbf{A}^x\partial_x\mathbf{u} + \mathbf{A}^z\partial_z\mathbf{u} + \mathbf{S} = 0, \tag{39}$$

where $\mathbf{u} = (\phi, \psi_v, \psi)^T$ is the state vector, and the principal matrices are given by

$$\begin{aligned}\mathbf{A}^u &= \mathrm{diag}(0,0,1),\\ \mathbf{A}^x &= \mathrm{diag}\left(1,1,\frac{-1}{2c_x}(1-x^2)^{3/2}\right),\end{aligned}$$

and

$$\mathbf{A}^z = \begin{pmatrix} 0 & 0 & 0\\ -1 & 0 & 0\\ 0 & 0 & -1\end{pmatrix}.$$

The source terms are denoted by S_ϕ, S_{ψ_v}, and S_ψ. The first two equations of (38) are intrinsic to a hypersurface of constant u, whereas the last is the "evolution equation" of the system. The angular principal part $\mathbf{A}^z$ is not diagonalizable, since it has a 2×2 Jordan block for the intrinsic equations, mimicking the core structure of the previously analyzed single-null PDEs. One may think of this model as a simplified analog of these systems with a compactified radial coordinate, similar to the way that the Bondi-Sachs formulation is used for characteristic extraction. This role can be played by the coordinate x with c_x a constant involved in the compactification. More specifically,

$$x = \frac{r - r_{\min}}{\sqrt{c_x^2 + (r - r_{\min})^2}},$$

where $r_{\min}$ is the minimum physical radius that we consider and the factor c_x controls the density of points toward $r \to \infty$, if we were to map the compactified grid x to the physical radius grid r.

By removing the angular derivative from the second intrinsic equation (38), we obtain our SH toy model:

$$\begin{aligned} \partial_x \phi &= -S_\phi, \\ \partial_x \psi_v &= -S_{\psi_v}, \\ \partial_u \psi - \frac{(1-x^2)^{3/2}}{2c_x}\partial_x \psi - \partial_z \psi &= -S_\psi, \end{aligned} \tag{40}$$

which has the same principal part matrices $\mathbf{A}^u$ and $\mathbf{A}^x$ as before but has diagonal $\mathbf{A}^z$. We employ this model for comparison between numerical results with SH and WH systems. The PDE problem for both systems (38) and (40) has as domain

$$x \in [0,1], \qquad z \in [0, 2\pi), \qquad u \in [u_0, u_f],$$

for some initial and final times u_0 and u_f, respectively. We apply periodic boundary conditions in the z direction for simplicity. The initial and boundary data are

$$\psi_* \equiv \psi(u_0, x, z) \tag{41}$$

and

$$\hat{\phi} \equiv \phi(u, 0, z), \qquad \hat{\psi}_v \equiv \psi_v(u, 0, z), \tag{42}$$

respectively, and are freely specifiable.

B. Algebraic determination of well posedness

So far, we have discussed the degree of hyperbolicity of GR in two gauges and constructed models that capture the basic structure we unearthed. As mentioned in the introduction, the reason we care about this algebraic characterization is that, in the linear constant-coefficient approximation, it determines well posedness of the initial value problem [13,29]. In this subsection, we present our well-posedness analysis, focusing on the WH toy model. The interested reader can find the complete analysis of both our models in Ref. [21]. In this analysis, we work in the constant-coefficient approximation, following closely the philosophy and notation of Ref. [29]. We start with the IVP and adjust our results to the CIBVP at the end. Specifically, we wish to understand what inequalities, with what norms, can be used to bound solutions in terms of their given data and how lower-order perturbations affect such estimates.

Consider the Cauchy problem for the linear, constant-coefficient system,

$$\partial_t \mathbf{u} = \mathbf{B}^p \partial_p \mathbf{u} + \mathbf{S} \equiv \mathbf{B}^p \partial_p \mathbf{u} + \mathbf{B}\mathbf{u}. \tag{43}$$

To be well posed in the L^2 norm, we must have real constants $K \geq 1$ and $\alpha \in \mathbb{R}$ such that

$$|e^{\mathbf{P}(i\omega)t}| \leq K e^{\alpha t}, \tag{44}$$

for all $t \geq 0$ and all $\omega \in \mathbb{R}^n$. Here

$$\mathbf{P}(i\omega) = i\omega_p \mathbf{B}^p + \mathbf{B} \tag{45}$$

is the constant-coefficient symbol of the PDE after Fourier transforming in space, with $i\omega_p \mathbf{B}^p$ the principal symbol and $\mathbf{B}\mathbf{u} = -\mathbf{S}$ the lower-order term related to sources. Essentially, inequality (44) states that the solution of the PDE has to be bounded at each time by an exponential that is independent of the Fourier mode ω_p. In this manner, we obtain an estimate of the solution $\mathbf{u}$ at all times by the initial data f:

$$\begin{aligned} ||\mathbf{u}(\cdot, t)||_{L^2} &= ||e^{\mathbf{P}(i\omega)t}\hat{f}(\omega)||_{L^2} \\ &\leq K e^{\alpha t}||\hat{f}||_{L^2} = K e^{\alpha t}||f||_{L^2}. \end{aligned}$$

In the terminology of Ref. [29], if a Cauchy problem instead satisfies only

$$|e^{\mathbf{P}(i\omega)t}| \leq K_1 e^{\alpha t}(1 + |\omega|^q), \tag{46}$$

with q some natural number, it is called weakly well posed. This type of estimate is weaker than (44), because the explicit appearance of ω on the right-hand side makes it impossible to bound the solution by an exponential independent of ω. If, rather than insisting on L^2, we allow also some *specific* derivative, determined by the system, within the norm, we can nevertheless obtain the estimate

$$||\mathbf{u}(\cdot, t)||_q \leq K_2 e^{\alpha t}||f||_q$$

for the solution $\mathbf{u}$. This would not be terrible, except that if the PDE is only weakly well posed, then perturbations to the system by generic lower-order terms will lead to

frequency-dependent exponential growth of the solution, and the resulting perturbed problem is ill posed in any sense. We show this explicitly for our WH models later. The latter is not true for well-posed problems, which remain well posed in the presence of lower-order perturbations [29,30].

To apply the above results directly, the system needs to be written in a form where the time principal part is the identity matrix. We achieve the latter via a coordinate transformation similar to those of Sec. II:

$$u = t - \rho, \qquad x = \rho, \qquad z = z.$$

Starting from Eqs. (38), we bring the system to the form

$$\begin{aligned}\partial_t \phi &= -\partial_\rho \phi - S_\phi,\\ \partial_t \psi_v &= -\partial_\rho \psi_v + \partial_z \phi - S_{\psi_v},\\ \partial_t \psi &= F\partial_\rho \psi + G\partial_z \psi - GS_\psi,\end{aligned}$$

where

$$F = \frac{(1-\rho^2)^{3/2}}{2c_x - (1-\rho^2)^{3/2}}, \qquad G = \frac{2c_x}{2c_x - (1-\rho^2)^{3/2}}$$

are fixed real constants for fixed ρ and c_x, with nonzero denominator for our ρ domain and an appropriately chosen c_x. In this frame, the principal parts are $\mathbf{B}^t = \mathbf{1}$ and

$$\mathbf{B}^\rho = \begin{pmatrix} -1 & 0 & 0\\ 0 & -1 & 0\\ 0 & 0 & F\end{pmatrix}, \qquad \mathbf{B}^z = \begin{pmatrix} 0 & 0 & 0\\ 1 & 0 & 0\\ 0 & 0 & G\end{pmatrix}.$$

This is the auxiliary Cauchy-type setup for the WH model, similarly to the PDEs in Sec. II after the coordinate transformation. After applying a Fourier transformation, the principal symbol for the WH model is

$$i\omega_p \mathbf{B}^p = i\omega_\rho \mathbf{A}^\rho + i\omega_z \mathbf{A}^z.$$

1. Homogeneous WH model

Focusing first on the homogeneous WH model where $S_\phi = S_{\psi_v} = S_\psi = 0$, we obtain

$$e^{(i\hat{\omega}_p \mathbf{B}^p)|\omega|t} = \begin{pmatrix} e^{-i|\omega|\hat{\omega}_\rho t} & 0 & 0\\ i|\omega|\hat{\omega}_z t e^{-i|\omega|\hat{\omega}_\rho t} & e^{-i|\omega|\hat{\omega}_\rho t} & 0\\ 0 & 0 & e^{i|\omega|(F\hat{\omega}_\rho + G\hat{\omega}_z)t}\end{pmatrix}, \tag{47}$$

where we express the wave vector as

$$\omega_p = |\omega|\hat{\omega}_p,$$

with $|\omega|$ its magnitude so that $\hat{\omega}_\rho^2 + \hat{\omega}_z^2 = 1$. The norm of (47) is (see Chap. 2 of Ref. [30] for useful definitions)

$$|e^{(i\hat{\omega}_p \mathbf{B}^p)|\omega|t}|^2 = 1 + \frac{|\omega|^2\hat{\omega}_z^2 t^2}{2} + \left[\left(1 + \frac{|\omega|^2\hat{\omega}_z^2 t^2}{2}\right)^2 - 1\right]^{1/2}. \tag{48}$$

This norm behaves as $|\omega|t$ for large $|\omega|$, and so the homogeneous WH model obeys an inequality of the form (46), with $q = 1$. Hence, this PDE is only weakly well posed and so satisfies an estimate in some $||\cdot||_q$ norm. This norm is specified for our system in Sec. III B 3. If one would discard from the previous analysis the equation for ψ_v of the homogeneous WH model (38), since it is decoupled, the remaining subsystem would be symmetric hyperbolic, and one might expect well posedness of the full system in the L^2 norm. However, as shown in Fig. 6, this expectation is not true.

2. Inhomogeneous WH model

For the homogeneous WH model, we computed the norm of $e^{(i\hat{\omega}_p \mathbf{B}^p)|\omega|t}$ to estimate the behavior of solutions. However, we could also examine the form of the eigenvalues of the full symbol $\mathbf{P}(i\omega)$ for large $|\omega|$ to understand if the solutions exhibit exponential growth in ω_p (see Lemma 2.3.1 of Ref. [29]). If there is any eigenvalue λ of $\mathbf{P}(i\omega)$ such that

$$\mathrm{Re}[\lambda] \sim |\omega|^s > 0 \quad \text{with} \quad s > 0,$$

for large $|\omega|$, then solutions of the PDE may exhibit frequency-dependent exponential growth, and the PDE problem is ill posed in any sense. For the inhomogeneous WH model, we consider the following possible lower-order source terms:

$$\mathbf{B}_1 = \begin{pmatrix} 0 & 0 & 1\\ 1 & 0 & 1\\ 1 & 0 & 0\end{pmatrix}, \quad \mathbf{B}_2 = \begin{pmatrix} 1 & 0 & 1\\ 1 & 1 & 1\\ 1 & 1 & 1\end{pmatrix}, \quad \mathbf{B}_3 = \begin{pmatrix} 0 & 1 & 0\\ 0 & 0 & 0\\ 0 & 0 & 0\end{pmatrix},$$

where $-\mathbf{S} = \mathbf{B}\mathbf{u}$. The choice $\mathbf{B}_1$ is motivated by analogy with the linearized Bondi-Sachs system with $\phi \sim \beta$, $\psi_v \sim V$, and $\psi \sim \gamma_r$. In $\mathbf{B}_2$, we include all possible source terms that do not break the nested structure of the intrinsic equations, and, finally, in choice $\mathbf{B}_3$ we introduce source terms that violate the nested structure, thus rendering the intrinsic system a coupled PDE. For both $\mathbf{B}_1$ and $\mathbf{B}_2$, the eigenvalues of $\mathbf{P}(i\omega)$ are

$$\lambda_1 = \lambda_2 = -i|\omega|\hat{\omega}_\rho, \qquad \lambda_3 = i|\omega|(F\hat{\omega}_\rho + G\hat{\omega}_z),$$

as $|\omega| \to \infty$, with the next terms appearing at the order of $|\omega|^0$. For these choices of lower-order source terms, the

inhomogeneous WH model remains well posed in the lopsided norm. On the other hand, if $\mathbf{B} = \mathbf{B}_3$, the eigenvalues of the symbol are

$$\lambda_1 = -i|\omega|\hat{\omega}_\rho - (-1)^{1/4}\sqrt{|\omega|\hat{\omega}_z} + O(|\omega|^0),$$
$$\lambda_2 = -i|\omega|\hat{\omega}_\rho + (-1)^{1/4}\sqrt{|\omega|\hat{\omega}_z} + O(|\omega|^0),$$
$$\lambda_3 = i|\omega|(F\hat{\omega}_\rho + G\hat{\omega}_z) + O(|\omega|^0)$$

for large $|\omega|$. Since $\mathrm{Re}[\lambda] \sim |\omega|^{1/2}$, we conclude that when the nested structure of the intrinsic equations is broken, the solution of the inhomogeneous WH exhibits frequency-dependent exponential growth. Consequently, the IVP with this system is no longer weakly well posed but ill posed. Note, in contrast, that for the homogeneous SH model we have

$$|e^{\mathbf{P}(i\omega)t}| = 1.$$

Hence, for this model, the IVP is well posed already in the L^2 norm. Unlike the WH model, well posedness for this model is not affected by source terms.

3. The CIBVP, CCE, and CCM

The previous analysis was performed in Fourier space and yielded that an IVP based on the homogeneous WH model may be well posed in an appropriate lopsided norm, whereas one on the SH model is (strongly) well posed in the L^2 norm. We now present our energy estimates for solutions to the IBVP and CIBVP by working in position space. For concreteness and simplicity, the PDE system for the IBVP is a homogeneous SH model (which is furthermore symmetric hyperbolic)

$$\partial_t\bar{\phi} + \partial_\rho\bar{\phi} + \partial_z\bar{\psi}_v = 0,$$
$$\partial_t\bar{\psi}_v + \partial_\rho\bar{\psi}_v + \partial_z\bar{\phi} = 0,$$
$$\partial_t\bar{\psi} - \frac{1}{2}\partial_\rho\bar{\psi} - \partial_z\bar{\psi} = 0, \tag{49}$$

with initial data $\bar{\phi}_*$, $\bar{\psi}_{v*}$, $\bar{\psi}_*$ on Σ_0, boundary data $\hat{\bar{\psi}}$ on $\mathcal{T}_0$ and domain $t \in [0, t_f]$, $\rho \in (-\infty, 0]$ and the compact $z \in [0, 2\pi)$, and for the CIBVP the homogeneous WH model

$$\partial_x\phi = 0, \tag{50a}$$
$$\partial_x\psi_v - \partial_z\phi = 0, \tag{50b}$$
$$\partial_u\psi - \frac{1}{2}\partial_x\psi - \partial_z\psi = 0, \tag{50c}$$

with initial data ψ_* on $\mathcal{N}_0$, boundary data $\hat{\phi}$ and $\hat{\psi}_v$ on $\mathcal{T}_0$ and domain $u \in [0, u_f], x \in [0, x_f]$ and the aforementioned z. The domains of the two problems are illustrated in Fig. 3. We view the IBVP as a simplified analog of GR in strongly (here even symmetric) hyperbolic formulations widely used in Cauchy-type problems, with the CIBVP standing for the Bondi-Sachs gauge used in characteristic evolutions. We wish to understand whether or not problems with these features can be successfully used for CCE or CCM in principle.

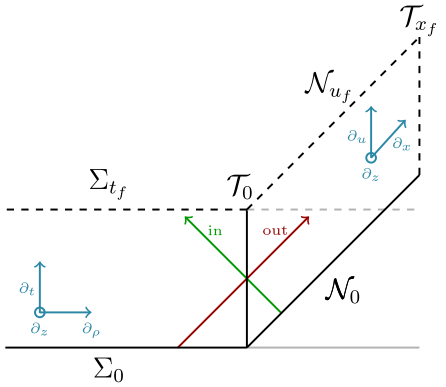

FIG. 3. The IBVP (left) and the CIBVP (right) setups. For CCE, outgoing data from the IBVP serve as boundary data on $\mathcal{T}_0$ for the CIBVP, which can be viewed as an independent PDE problem. In this case, the IBVP's spatial domain is more extended such that data on $\mathcal{T}_0$ are unaffected by the boundary conditions chosen for the problem. For CCM, the IBVP and CIBVP are solved simultaneously and out- and ingoing data are communicated from one to the other via $\mathcal{T}_0$. Effectively, the two problems are viewed as one.

For the IBVP estimate, our starting point is

$$\partial_t\|\bar{\mathbf{u}}\|^2_{L^2(\Sigma_t)} = \partial_t\int_{\Sigma_t}\bar{\mathbf{u}}^T\bar{\mathbf{u}} = \partial_t\int_{\Sigma_t}(\bar{\phi}^2 + \bar{\psi}_v{}^2 + \bar{\psi}^2),$$

which after using (49), the divergence theorem assuming $\bar{\mathbf{u}} \to \mathbf{0}$ as $\rho \to -\infty$, and integrating in the t domain, yields

$$\|\bar{\mathbf{u}}\|^2_{L^2(\Sigma_{t_f})} + \|\bar{\mathbf{u}}\|^2_{L^2_{\mathrm{out}}(\mathcal{T}_0)} = \|\bar{\mathbf{u}}\|^2_{L^2(\Sigma_0)} + \|\bar{\mathbf{u}}\|^2_{L^2_{\mathrm{in}}(\mathcal{T}_0)}, \tag{51}$$

where $\|\bar{\mathbf{u}}\|^2_{L^2_{\mathrm{out}}(\mathcal{T}_0)}$ denotes the integral over $\mathcal{T}_0$ that contains only the outgoing fields $\bar{\phi}$ and $\bar{\psi}_v$, and similarly for the ingoing. The estimate (51) states that the energy of the solution equals the energy of its given data, so that the solution is controlled by the given data.

In a Cauchy-type setup, we specify all fields on the initial spacelike hypersurface, and, by solving the system, we obtain all of them on spacelike hypersurfaces to the future. On the contrary, in a single-null characteristic setup, fields with "evolution" equations are chosen on the initial null hypersurface, and those that satisfy equations intrinsic to the null hypersurfaces are specified as boundary data. As we will see in the following, this has a natural consequence on the type of estimates that we can hope to demonstrate, in terms of both the domain on which we integrate and the

particular fields that appear. This is due to the geometry of the setup.

Motivated from the IVP estimates in Fourier space of Secs. III B 1 and III B 2, we might naively first consider for the CIBVP the *lopsided norm*

$$\|\mathbf{u}\|^2_{q(\mathcal{D})} = \int_{\mathcal{D}} (\phi^2 + \psi_v^2 + \psi^2 + (\partial_z \phi)^2),$$

in some domain $\mathcal{D}$, where only $\partial_z \phi$ is added to the integrand of the L^2 norm, because precisely this term causes the pathological structure in the angular principal part of the WH model. Following our previous discussion, however, it is more appropriate to split the integrand into separate pieces for the ingoing and outgoing variables. The domain $\mathcal{D}$ becomes $\mathcal{N}_u$ and $\mathcal{T}_x$, respectively, for each. For the ingoing variables, we start from

$$\partial_u \|\mathbf{u}\|^2_{q_{\rm in}(\mathcal{N}_u)} = \partial_u \int_{\mathcal{N}_u} \psi^2,$$

since there are no ∂_u equations for the outgoing ones. We assume that $\psi \to 0$ as $x \to x_f$ in the given data, which is the analog in our model to requiring no incoming gravitational waves from future null infinity, working on a compactified radial domain. After using (50c), the divergence theorem and integrating in the u domain, we obtain

$$2\|\mathbf{u}\|^2_{q_{\rm in}(\mathcal{N}_{u_f})} + \|\mathbf{u}\|^2_{q_{\rm in}(\mathcal{T}_0)} = 2\|\mathbf{u}\|^2_{q_{\rm in}(\mathcal{N}_0)}. \tag{52}$$

For the outgoing variables, the starting point is

$$\partial_x \|\mathbf{u}\|^2_{q_{\rm out}(\mathcal{T}_x)} = \partial_x \int_{\mathcal{T}_x} (\phi^2 + \psi_v^2 + (\partial_z \phi)^2),$$

and, by using (50a) and (50b), the divergence theorem and integrating in the x domain up to some arbitrary x', we obtain

$$\|\mathbf{u}\|^2_{q_{\rm out}(\mathcal{T}_{x'})} = \|\mathbf{u}\|^2_{q_{\rm out}(\mathcal{T}_0)} + \int_0^{x'} \left(\int_{\mathcal{T}_x} 2\psi_v \partial_z \phi \right) dx, \tag{53}$$

where the last term is due to the hyperbolicity of the system and would not appear for our SH example. Using $2\psi_v \partial_z \phi \le \phi^2 + \psi_v^2 + (\partial_z \phi)^2$, the latter reads

$$\|\mathbf{u}\|^2_{q_{\rm out}(\mathcal{T}_{x'})} \le \|\mathbf{u}\|^2_{q_{\rm out}(\mathcal{T}_0)} + \int_0^{x'} \|\mathbf{u}\|^2_{q_{\rm out}(\mathcal{T}_x)} dx,$$

and by applying Grönwall's inequality we obtain

$$\|\mathbf{u}\|^2_{q_{\rm out}(\mathcal{T}_{x'})} \le e^{x'} \|\mathbf{u}\|^2_{q_{\rm out}(\mathcal{T}_0)}. \tag{54}$$

Hence, the energy of the outgoing fields at each arbitrary timelike hypersurface $\mathcal{T}_{x'}$ in the characteristic domain is bounded. The sum of Eqs. (52) and (54) is the complete energy estimate for the CIBVP and yields

$$\begin{aligned} &2\|\mathbf{u}\|^2_{q_{\rm in}(\mathcal{N}_{u_f})} + \|\mathbf{u}\|^2_{q_{\rm in}(\mathcal{T}_0)} + \sup_{x'} \|\mathbf{u}\|^2_{q_{\rm out}(\mathcal{T}_{x'})} \\ &\quad \le 2\|\mathbf{u}\|^2_{q_{\rm in}(\mathcal{N}_0)}|^2_{||} + e^{x_f} \|\mathbf{u}\|^2_{q_{\rm out}(\mathcal{T}_0)}, \end{aligned} \tag{55}$$

where we used that $e^{x'} \le e^{x_f}$ for $x' \in [0, x_f]$ and chose the supremum of $\|\mathbf{u}\|^2_{q_{\rm out}(\mathcal{T}_{x'})}$ to obtain the largest possible bounded left-hand side, since the outgoing lopsided norm is not necessarily monotonically increasing with x. Thus, the energy of the solution to the CIBVP is controlled by the given data on $\mathcal{N}_0$ and $\mathcal{T}_0$.

We first interpret these estimates in the framework of CCE. Choosing suitable data, our estimate for the IBVP shows that one obtains a smooth solution in the domain of the Cauchy-type setup. One can then use this solution to provide boundary data on $\mathcal{T}_0$ for the CIBVP that are finite also in the lopsided norm, and the solution to this characteristic problem has a good energy estimate as shown earlier, too. Hence, the CCE process is perfectly valid for our model and, provided analogous estimates for GR in the Bondi-like gauges used, would be in that context, too. One question that arises for GR, but which for now we have no insight, is whether or not this procedure excludes any data of interest. For CCM, the discussion is rather different, since IBVP and CIBVP are solved simultaneously and data are communicated between domains. Effectively, one joins the PDE problems, and they may be viewed as one. Hence, let us try to obtain an energy estimate for the joint PDE problem, by adding Eqs. (51) and (55):

$$\begin{aligned} &\|\mathbf{u}\|^2_{L^2(\Sigma_{t_f})} + \|\mathbf{u}\|^2_{L^2_{\rm out}(\mathcal{T}_0)} + 2\|\mathbf{u}\|^2_{q_{\rm in}(\mathcal{N}_{u_f})} \\ &\quad + \|\mathbf{u}\|^2_{q_{\rm in}(\mathcal{T}_0)} + \sup_{x'} \|\mathbf{u}\|^2_{q_{\rm out}(\mathcal{T}_{x'})} \\ &\le \|\mathbf{u}\|^2_{L^2(\Sigma_0)} + \|\mathbf{u}\|^2_{L^2_{\rm in}(\mathcal{T}_0)} + 2\|\mathbf{u}\|^2_{q_{\rm in}(\mathcal{N}_0)} + e^{x_f} \|\mathbf{u}\|^2_{q_{\rm out}(\mathcal{T}_0)}, \end{aligned} \tag{56}$$

where now $\bar{u} = \mathbf{u}$. For the joint problem there is "effectively" no boundary $\mathcal{T}_0$ at which we are free to choose data, and, hence, any estimate should not involve integrals over this domain. The relevant terms can, however, cancel each other only if the two norms that appear coincide. This requires either that the CIBVP relies on a symmetric hyperbolic PDE system and, hence, is well posed in the L^2 norm (see, for instance, [31–33]) or that the IBVP relies on a system that is well posed in the same lopsided norm as the CIBVP. But this requires special structure, above and beyond symmetric hyperbolicity, on the equations used in the IBVP. Regarding GR, the first option would translate into developing a SH (hopefully also symmetric hyperbolic) single-null formulation and the second to building a formulation that is well posed in the same lopsided norm that Bondi-like gauges (perhaps) are. Given the long search

for formulations that *work* for practical evolution, however, such an artisanal construction seems poorly motivated. In summary, unless special structure is present in the field equations solved for the IBVP, the solution to the weakly hyperbolic CIBVP cannot be combined with that of an IBVP of a symmetric hyperbolic system in such a way as to provide a solution to the whole problem which has an energy bounded by that of the given data.

IV. NUMERICAL EXPERIMENTS

We now use the toy models introduced in Sec. III to diagnose the effects of weak hyperbolicity at the numerical level. We perform convergence tests in the single-null setup for both the WH and SH models in a discrete approximation to the L^2 norm, for smooth and noisy given data. We also perform convergence tests with noisy given data in the lopsided norm, for the different versions of the WH model analyzed in the previous section.

A. Implementation

As in other schemes to solve the CIBVP, several different ingredients are needed in the algorithm. These can be summarized for our models (38) and (40) as follows.

(1) The domain of the PDE problem is $x \in [0,1]$, $z \in [0, 2\pi)$ with periodic boundary conditions and $u \in [u_0, u_f]$, with u_0 and u_f the initial and final times, respectively. We always include the point $x = 1$ in the computational domain so that we do not need to impose boundary conditions at the outer boundary, since there are no incoming characteristic variables there.
(2) For the initial time u_0, provide initial data $\psi(u_0, x, z)$ on the surface $u = u_0$ and boundary data $\phi(u_0, 0, z)$ and $\psi_v(u_0, 0, z)$.
(3) Integrate the intrinsic equations of each model to obtain $\phi(u_0, x, z)$ and $\psi_v(u_0, x, z)$. We perform this integration using the two-stage, second-order strong stability preserving method of Shu and Osher (SSPRK22) [34].
(4) Integrate the evolution equation of each model to obtain $\psi(u_1, x, z)$ at the surface $u = u_1 = u_0 + \Delta u$. We choose $\Delta u = 0.25\Delta x$ to satisfy the Courant-Friedrichs-Lewy (CFL) condition, and the numerical integration is performed using the fourth-order Runge-Kutta (RK4) method.
(5) Any derivative appearing in the right-hand sides of these integrations is approximated using second-order accurate centered finite difference operators, except at the boundaries, where second-order accurate forward and backward difference operators are used, respectively.
(6) Providing boundary data $\phi(u, 0, z)$ and $\psi_v(u, 0, z)$ as in the PDE specification (42), we repeat steps 2 and 3 to obtain $\phi(u, x, z)$, $\psi_v(u, x, z)$ and $\psi(u, x, z)$ until the final time u_f. This is the solution of the PDE.

No artificial dissipation is introduced. The implementation was made using the Julia language [35] with the DifferentialEquations.jl package [36] to integrate the equations. Our code is freely available [21]. We apply convergence tests to our numerical scheme for both toy models. The tests are performed for smooth, as well as for noisy given data. The latter are often called robust stability tests. They form part of the Mexico-city test bed for numerical relativity [37]. These tests have been performed widely in the literature [38–43], often, as in our case, with adaptations for the setup under consideration.

B. Convergence tests

By *convergence,* we mean the requirement that the difference between the numerical approximation provided by a finite difference scheme and the exact solution of the continuum PDE system tends to zero as the grid spacing is increased. The finite difference scheme is called *consistent* when it approximates the correct PDE system, and the degree to which this is achieved is its *accuracy*. The scheme is called *stable* if it satisfies a discretized version of (44) or (46). In this context, versions of each continuum norm are replaced by a suitable discrete analog. Here we replace the L^2 norm for the single-null setup with

$$\|\mathbf{u}\|^2_{h_u,h_x,h_z} = \sum_{x,z} \psi^2 h_x h_z + \max_x \sum_{u,z} (\phi^2 + \psi_v^2) h_u h_z, \quad (57)$$

with the first sum taken over all points on the grid, with h_x and h_z the grid spacing in the x and z directions, respectively, and the second sum over all points in the z and u directions ($h_u = 0.25 h_x$ for our setup), for all x grid points and keeping the maximum in the x direction. The first sum involves only ingoing and the second only outgoing variables. When, as will be the case in what follows, we have $h_x = h_z = h$, we label the norm simply with h. Our discrete approximation to the lopsided norm is

$$\|\mathbf{u}\|^2_{|^2_{q(h_u,h_x,h_z)}} = \sum_{x,z} \psi^2 h_x h_z + \max_x \sum_{u,z} (\phi^2 + \psi_v^2 + (D_z\phi)^2) h_u h_z, \quad (58)$$

where D_z is the second-order accurate, centered, finite difference operator that replaces the continuum operator ∂_z, by

$$D_z f_h(x_i) = \frac{f_h(x_{i+1}) - f_h(x_{i-1})}{2h_z}, \quad (59)$$

for a grid function f_h on a grid with spacing h_z. When the two grid spacings are equal, we again label the norm simply

with h. This approximation to the continuum lopsided norm is not unique. If we were attempting to prove that a particular discretization converged, it might be necessary to take another. Denoting by f the solution to the continuum system and as f_h the numerical approximation at resolution h provided by a convergent finite difference scheme of accuracy n, then

$$f = f_h + O(h^n), \tag{60}$$

and, hence,

$$\|f - f_h\| = O(h^n), \tag{61}$$

in some appropriate norm $\|\cdot\|$ on the grid, with the understanding that the exact solution should be evaluated on said grid. Full definitions of the notions of consistency, stability, and convergence for the IVP can be found, for example, in Refs. [13,39,44].

We use a second-order accurate numerical approximation, so that $n = 2$. Considering numerical evolutions with coarse, medium, and fine grid spacings h_c, h_m, and h_f, respectively, we can construct a useful quantity for these tests:

$$Q \equiv \frac{h_c^n - h_m^n}{h_m^n - h_f^n}, \tag{62}$$

which we call *convergence factor*. In our convergence tests, we solve the same discretized PDE problem for different resolutions, and every time we want to increase resolution we halve the grid spacing in all directions, i.e.,

$$h_m = h_c/2, \qquad h_f = h_c/4.$$

Following this approach, the convergence factor is $Q = 4$. Combining (60) and (62), one can obtain the relation

$$f_{h_c} - f_{h_c/2} = Q(f_{h_c/2} - f_{h_c/4}), \tag{63}$$

understood on shared grid points in the obvious way, which is used to investigate pointwise convergence. In what follows, the different resolutions are denoted as

$$h_q = h_0/2^q.$$

The lowest resolution h_0 has $N_x = 17$ points in the x grid and $N_z = 16$ in the z grid. We work in units of the code in the entire section.

1. Smooth data

For the simulations with smooth given data, the initial and final times are $u_0 = 0$ and $u_f = 1$, respectively. For both toy models, we provide as initial data

$$\psi(0, x, z) = e^{-100(x-1/2)^2}\sin(z)$$

and as boundary data

$$\phi(u, 0, z) = 3e^{-100(u-1/2)^2}\sin(z)$$

and

$$\psi_v(u, 0, z) = e^{-100(u-1/2)^2}\sin(z).$$

For the SH model, we choose the following source terms:

$$-S_\phi = \psi, \qquad -S_{\psi_v} = \phi + \psi, \qquad -S_\psi = \phi, \tag{64}$$

and for the WH model we choose the homogeneous case. As discussed in Sec. III B, well posedness of the SH model is unaffected by lower-order source terms, so the specific choice of source terms here is not vital. However, we choose to work with the homogeneous WH model, because weakly well-posed problems are sensitive to lower-order perturbations.

Runs with resolutions h_0, h_1, h_2, h_3, h_4, and h_5 were performed. In Fig. 4, the basic dynamics are plotted with each model. To first verify that the numerical scheme is implemented successfully, we performed pointwise convergence tests for both models. We focus specifically here on the highest three resolutions. The algorithm is the following:

(1) Consider h_3, h_4, and h_5 as coarse, medium, and fine resolutions, respectively.
(2) Calculate $\psi_{h_3} - \psi_{h_4}$ and $\psi_{h_4} - \psi_{h_5}$ for the grid points of h_3, for the final time step of the evolution.
(3) Plot simultaneously $\psi_{h_3} - \psi_{h_4}$ and $Q(\psi_{h_4} - \psi_{h_5})$. As indicated from (63), for a convergent numerical scheme the two quantities should overlap, when multiplying the latter with the appropriate convergence factor.

In Fig. 5, we illustrate the results of this test for the aforementioned smooth given data for both models. At this resolution, one clearly observes perfect pointwise convergence in both cases.

We also wish to examine convergence of our numerical solutions in discrete approximations of the aforementioned norms. Given that the exact solution to the PDE problem is unknown and that each time we increase resolution we decrease the grid spacing in all directions by a factor of d, we can build the following useful quantity:

$$\mathcal{C}_{\text{self}} = \log_d \frac{\|\mathbf{u}_{h_c} - \perp_{h_c}^{h_c/d}\mathbf{u}_{h_c/d}\|_{h_c}}{\|\perp_{h_c}^{h_c/d}\mathbf{u}_{h_c/d} - \perp_{h_c}^{h_c/d^2}\mathbf{u}_{h_c/d^2}\|_{h_c}}, \tag{65}$$

which we call the *self-convergence ratio*, with $\mathbf{u} = (\phi, \psi_v, \psi)^T$ the state vector of the PDE system and ϕ, ψ_v, and ψ grid functions. Here $\perp_{h_c}^{h_c/d}$ denotes the projection

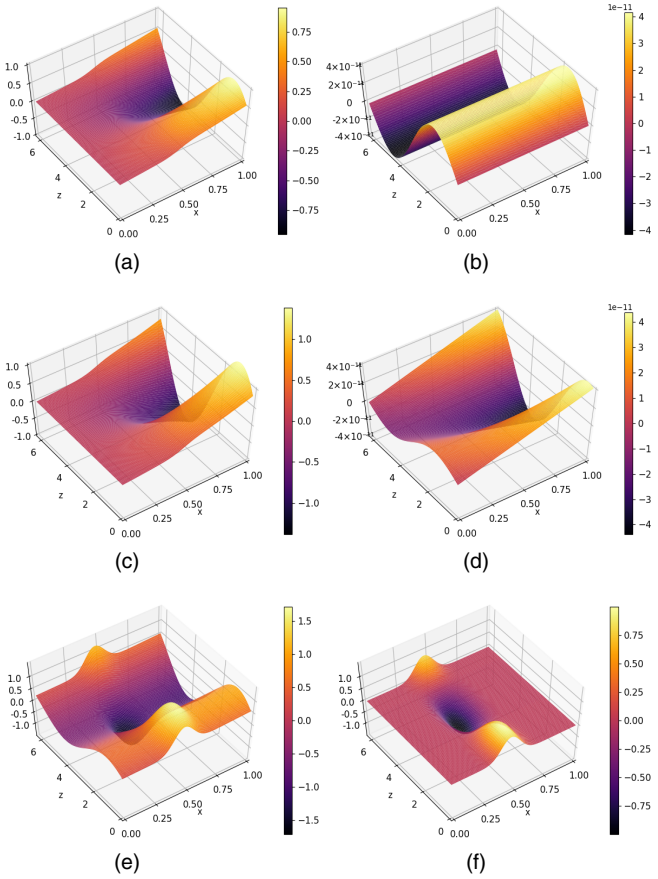

FIG. 4. The fields ϕ, ψ_v, and ψ at final evolution time $u = 1$, for the SH model (left) and the homogeneous WH model (right), with the same smooth given data. Observe that the fields ϕ and ψ_v in the WH case are still of the same magnitude $\sim 10^{-11}$ as the boundary data at the retarded time $u = 1$. This is not true once generic source terms are taken.

(in our setup injection) operator from the h_c/d grid onto the h_c grid. We calculate $\mathcal{C}_{\text{self}}$ for a discrete analog of the L^2 norm. However, if one wishes to examine convergence in a different norm, L^2 can be replaced with that. The theoretical value of $\mathcal{C}_{\text{self}}$ equals the accuracy n of the numerical scheme, and in our specific setup

$$\mathcal{C}_{\text{self}} = \log_2 \frac{\|\mathbf{u}_{h_c} - \perp_{h_c}^{h_c/2} \mathbf{u}_{h_c/2}\|_{h_c}}{\|\perp_{h_c}^{h_c/2} \mathbf{u}_{h_c/2} - \perp_{h_c}^{h_c/4} \mathbf{u}_{h_c/4}\|_{h_c}} = 2. \tag{66}$$

We obtain numerical solutions for the same smooth given data for both models at the various resolutions mentioned before. For triple resolution, double resolution, and quadruple resolution, we project all grid functions onto the coarse grid, and compute C_{self} at its time steps. In the left panel in Fig. 6, we collect the results of these norm convergence tests. Both models show similar behavior. At low resolutions, the curve drifts from the desired rate at early times, but the situation improves as we increase resolution, with C_{self} approaching the expected value. The

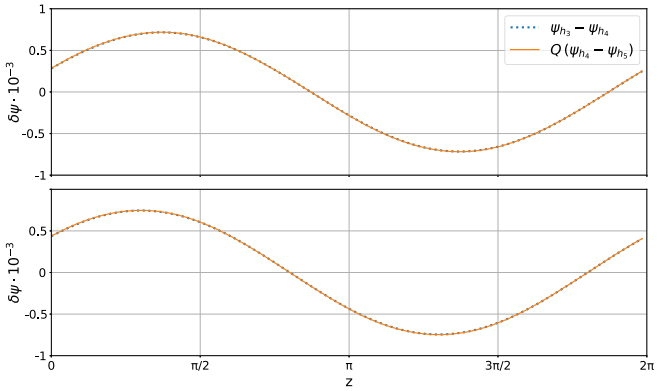

FIG. 5. Here we plot simultaneously $\psi_{h_3} - \psi_{h_4}$ and $Q(\psi_{h_4} - \psi_{h_5})$, for the SH (top) and the WH (bottom) toy models. We fix $x = 0.5$. Since our scheme is second order and we are doubling resolution, we fix $Q = 4$. The results for fixed z are similar. The plot is compatible with perfect second-order pointwise convergence.

trend with increasing resolution is the essential behavior we are looking at in these tests. By limiting ourselves to convergence tests with smooth given data, we could be misled that the WH toy model provides a well-posed CIBVP in the L^2 norm, since the numerical solutions appear to converge in this norm during our simulations. In other words, were we ignorant of the hyperbolicity of the system, it would be impossible to distinguish strongly and weakly hyperbolic PDEs with this test.

2. Noisy data

One can also perform norm convergence tests with random noise as given data, which is a strategy to simulate numerical error in an exaggerated form. Since it is expected that numerical error decreases as resolution increases, when performing simulations for these tests, one must scale appropriately the amplitude of the noise as resolution improves. This scaling is important to construct a sequence of initial data that converges in a suitable norm to initial data appropriate for the continuum system. The choice of norm here is essential and should be one which, if possible, provides a bound for the solution of a (weakly) well-posed PDE problem, in the sense of (44) and (46).

For these tests, we perform simulations where the smooth part of the given data is trivial (zero), and, hence, the exact solution for every PDE problem based on our models vanishes identically. Knowing the exact solution, in addition to the self-convergence rate (65), we can also construct the exact convergence ratio

$$\mathcal{C}_{\text{exact}} = \log_d \frac{\|\mathbf{u}_{h_c} - \mathbf{u}_{\text{exact}}\|_{h_c}}{\|\perp_{h_c}^{h_c/d} \mathbf{u}_{h_c/d} - \mathbf{u}_{\text{exact}}\|_{h_c}}, \tag{67}$$

where we decrease grid spacing by a factor of d when increasing resolution. $\mathcal{C}_{\text{exact}}$ is cheaper numerically

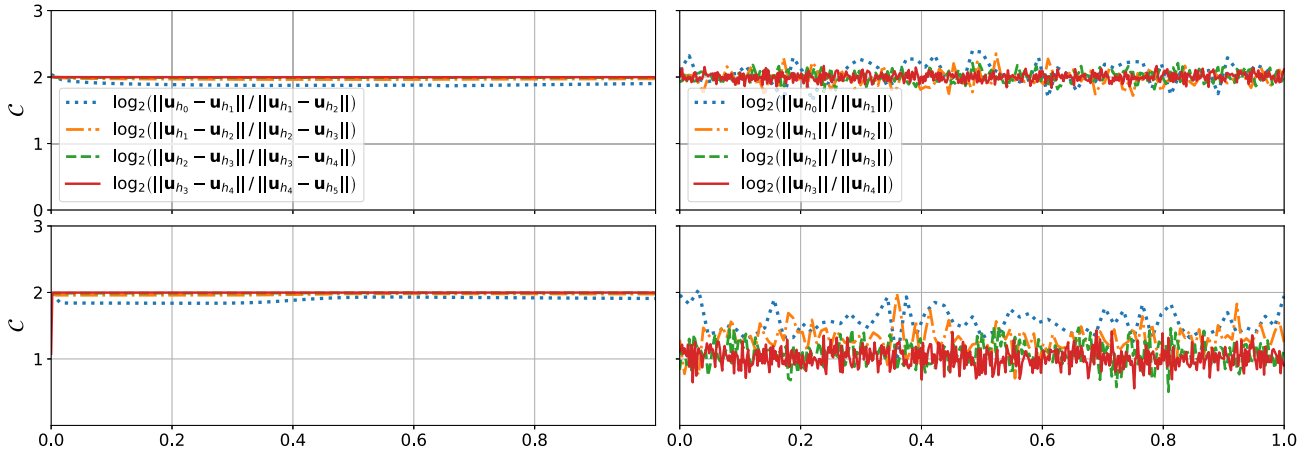

FIG. 6. The convergence ratio in the L^2 norm, for the strongly (above) and the weakly (below) toy models, for smooth (left) and noisy (right) given data, as a function of the simulation time. All plots have the same scale on the y axis. For smooth given data, we consider the self-convergence ratio (66), while, for noisy given data, the exact convergence ratio (67). If we consider the self-convergence ratio also for the noisy case, the results are qualitatively the same.

than $\mathcal{C}_{\text{self}}$, since only two different resolutions are required to build it, and again the exact solution is understood to be evaluated on the grid itself. It is possible for a scheme to be self-convergent but fail to be convergent, for example, if one were to implement the wrong field equations in error. Therefore, one would like to compare the numerical solution to an exact solution wherever (rarely) possible. To calculate $\mathcal{C}_{\text{exact}}$, we compute the discretized approximation to a suitable continuum norm at two resolutions, one twice the other. Each are computed on the naturally associated grid. We then take the ratio of the two at shared time steps, corresponding to those of the coarse grid h_c. In our setup $\mathbf{u}_{\text{exact}} = \mathbf{0}$ and $d = 2$; hence,

$$\mathcal{C}_{\text{exact}} = \log_2 \frac{\|\mathbf{u}_{h_c}\|_{h_c}}{\|\perp_{h_c}^{h_c/2}\mathbf{u}_{h_c/2}\|_{h_c}}, \tag{68}$$

which again equals two for perfect convergence. As previously mentioned, appropriate scaling of the random noise amplitude is crucial and is determined by the norm in which we wish to test convergence. To realize the proper scaling in our setup, let us consider the exact convergence ratio (68) and denote as A_{h_c} and $A_{h_c/2}$ the amplitude of the random noise for simulations with resolution h_c and $h_c/2$, respectively:

$$\mathcal{C}_{\text{exact}} = \log_2 \frac{\|\mathbf{u}_{h_c}\|_{h_c}}{\|\perp_{h_c}^{h_c/2}\mathbf{u}_{h_c/2}\|_{h_c}} \sim \log_2 \frac{O(A_{h_c})}{O(A_{h_c/2})}.$$

The above suggests that, to construct noisy data that converge in the discretized version of the L^2 norm (57) for our second-order accurate numerical scheme, we need to drop the amplitude of the random noise by a quarter every time we double resolution. For convergence tests in the lopsided norm, the scaling factor is different, due to the $D_z\phi$ term that appears in the discretized version of the lopsided norm (58). By replacing the L^2 with the lopsided norm in (68), we get

$$\mathcal{C}_{\text{exact}} = \log_2 \frac{\|\mathbf{u}_{h_c}\|_{q(h_c)}}{\|\perp_{h_c}^{h_c/2}\mathbf{u}_{h_c/2}\|_{q(h_c)}} \sim \log_2 \frac{O(A_{h_c})}{2O(A_{h_c/2})},$$

where now the norm estimate is dominated by the $D_z\phi$ term. Hence, to construct noisy data that converge in the lopsided norm for our second-order accurate numerical scheme, we need to multiply the amplitude of the random noise with a factor of one-eighth every time we double resolution. This discussion would be more complicated if we were using either pseudospectral approximation or some hybrid scheme, which is why we focus exclusively on a straightforward finite differencing setup.

The results for norm convergence tests with appropriately scaled noisy data for the L^2 norm, for both SH and WH models, are collected in the right column in Fig. 6. As illustrated there, the inhomogeneous SH model still exhibits convergence, since with increasing resolution the exact convergence ratio tends closer to the desired value of two at all times of the evolution. On the contrary, the homogeneous WH model does not converge, and it becomes clear that with increasing resolution the exact convergence ratio of this model moves further away from two at all times.

To appreciate *intuitively* why noisy data allow us to diagnose a lack of strong hyperbolicity, consider the systems in frequency space as in Sec. III B, which we may think of as momentum space. In practical terms, Eq. (48) states that the homogeneous WH model does not satisfy condition (44), and so high-frequency modes can grow arbitrarily fast. Considering smooth data, however, predominantly low-frequency modes are excited, and so

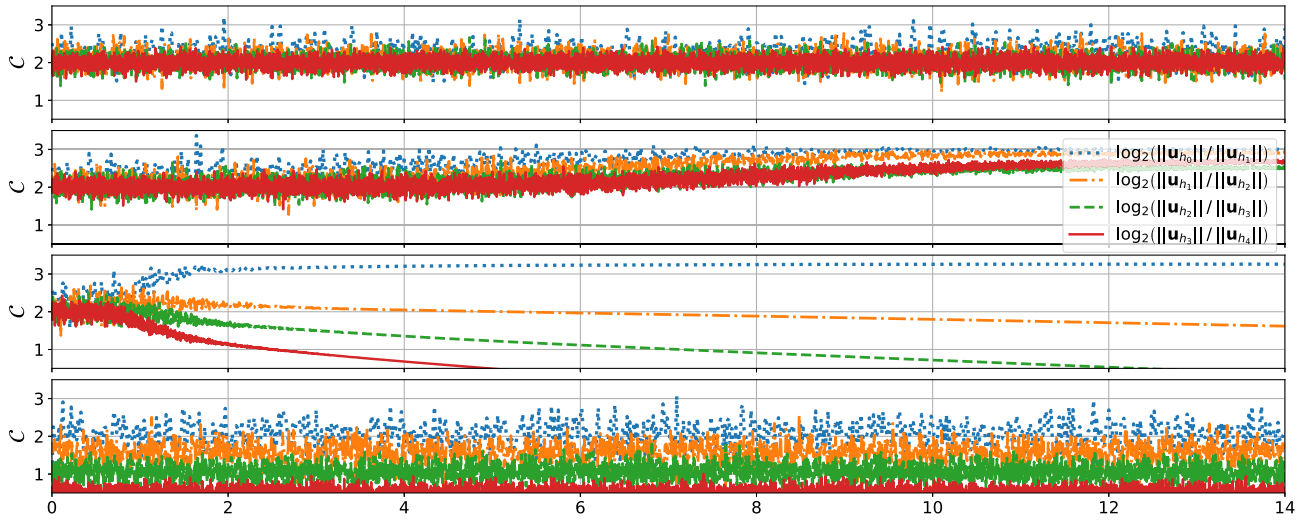

FIG. 7. The exact convergence ratio in the lopsided norm (58) for the different WH models. From top to bottom, we plot the homogeneous WH model, and then the inhomogeneous adjustments, in order B_1, B_2, and B_3. Overall, we conclude that the homogeneous model and B_1 models are converging in the limit of infinite resolution, with the others failing to do so. Of these, all but the third panel, with source B_2, agree with our expectation from continuum considerations. In this one case, our method appears to have an honest numerical instability, which could be understood properly by careful consideration of the scheme.

using our discretized approximation the violation of inequality (44) is not visible at the limited resolutions we employ. Noisy data, on the contrary, excite substantially both high- and low-frequency modes, with the former crucial to illustrate the violation.

We also perform convergence tests in the lopsided norm (58) to examine the behavior of the different WH models. As in the previous setup, in these tests we monitor the exact convergence ratio as a function of the simulation time. As illustrated in Fig. 7, our expectations from Sec. III B for the homogeneous model are verified. The homogeneous WH model converges at all times in the lopsided norm, provided, of course, that the given data are restricted to converge at second order to the trivial solution in the same norm. As also expected, the inhomogeneous case with B_3 fails to converge whatsoever during the evolution, exhibiting behavior similar to the homogeneous WH model in the L^2-norm tests. In fact, in this test the exact convergence ratio diverges further from two with increasing resolution and at earlier times. The discussion for the inhomogeneous WH models with sources B_1 and B_2 is more subtle. Both cases initially exhibit convergence, with the B_1 case maintaining this behavior for longer. The difference lies in their late time behavior and their trend with increasing resolution. In particular, the B_1 case converges for longer with increasing resolution, whereas B_2 does the opposite. At late times, in the B_1 case, $\mathcal{C}_{\text{exact}}$ reaches a plateau that converges to two with increasing resolution, which is not true with sources B_2. Thus, our numerical evidence seems to indicate that the B_1 inhomogeneous WH model converges in the lopsided norm but to disagree with the theoretical expectation at the continuum that the B_2 case does so, too. This is not in contradiction with our earlier calculations, however, because, as a careful examination of the approximation could reveal, purely algorithmic shortcomings may render a scheme nonconvergent.

V. CONCLUSIONS

Single-null formulations of GR are popular for applications in numerical relativity in various settings. In asymptotically flat spacetimes, they are used with compactified coordinates to compute gravitational waveforms at future-null infinity. In asymptotically AdS spacetimes, they are used to compute *in* from the timelike conformal boundary. But relatively little attention has been paid to well posedness of the resulting PDE problems, which serves as an obstacle to the construction of rigorous error estimates from computational work. Presently, therefore, we have examined two popular formulations, the Bondi-Sachs and affine-null systems, and performed numerical tests for toy models that illustrate the relevance of our findings. We found in a free-evolution analysis that, due to the nondiagonalizability of their angular principal part matrices, both are only weakly hyperbolic.

Our analysis employed a first-order reduction but was sufficiently general to rule out the existence of any other reduction (at least within a large class) that is strongly hyperbolic. We showed also that the degeneracy cannot be avoided by a change of frame. Textbook results on these systems then show that they are ill posed in the L^2 norm or its obvious derivatives. Considering model problems of a similar structure, we saw that the same result naturally carries over to the CIBVP. In the latter case, care is needed not to confuse the usual degeneracy of the norms that appear naturally in characteristic problems with high-frequency

blowup of solutions. It follows that a numerical approximation cannot converge to the exact solution of these PDE problems in any discrete approximation to L^2. We demonstrated this shortcoming numerically using our models and adapting the well-known robust-stability test. Spotting this shortcoming in practice is subtle, because smooth data may, and often do, give misleading results.

Although our weakly hyperbolic toy model is ill posed in L^2, it may be well posed in a lopsided norm in which the angular derivative of some specific components of the state vector are included. Thus, in such a case one must be able to control the size of not only the elements of the state vector in the given data, but also some of their derivatives. This weaker notion of well posedness is sensitive to the presence of lower-order source terms. For example, our weakly hyperbolic model is well posed in a (specific) lopsided norm if it is homogeneous, or inhomogeneous with sources that respect the nested structure of the equations intrinsic to the characteristic hypersurfaces. If this nested structure is broken by the source terms, it becomes ill posed in any sense. Again using random noise for initial data, our numerical experiments are consistent with this analytic result. There is one case in which convergence is not apparent in our approximation, despite the well posedness of the continuum equations in the lopsided norm. This is our only example of a *pure* numerical instability and is important, as it highlights the fact that for weakly hyperbolic systems numerical methods are not well developed and are not guaranteed to converge, even when using lopsided norms.

Bringing our attention back to the characteristic initial boundary value problem for GR, which covers both CCE and applications in numerical holography, it is clear that the two formulations we considered will be ill posed in L^2. It is not clear, however, in general, if they will admit estimates in suitable lopsided norms. But since the field equations *do* have a nested structure, and our weakly hyperbolic model problem turned out to admit estimates in lopsided norms whenever this structure was present, there is reason to be hopeful. On the other hand, given this uncertainty and the fact that numerical approximation to weakly hyperbolic systems (using lopsided norms) is poorly understood, it is desirable to obtain and adopt strongly or ideally symmetric hyperbolic alternatives. These could be sought out by changing gauge directly or by the use of a dual-foliation formulation as suggested in Ref. [26]. Perhaps a simpler option would be to pay the price of evolving curvature quantities as variables. Several such formulations are known to be symmetric hyperbolic in a double-null gauge [45–47] and could be adjusted appropriately.

A true *principle* solution to wave extraction would be a robust scheme for CCM, the other main alternative being the use of compactified hyperboloidal slices, a topic also under active research for full GR [48–57]. To understand the consequences of our findings for CCM, we considered a model in which the IBVP is solved for a symmetric hyperbolic system, and the solutions are then glued through boundary conditions to those of a weakly hyperbolic system accepting estimates in lopsided norms. The former of these two sets of equations is viewed as a model for the formulation used in the strong-field region, the latter for a single-null formulation used on the outer characteristic domain. With this setup, we found that the fundamental incompatibility of the norms naturally associated with the two domains prohibits their combined use in building estimates. But if the weakly hyperbolic system were made symmetric, hyperbolic progress could be made. A less appealing possibility would be to demonstrate that the formulation in the Cauchy domain, or some suitable replacement, admits estimates in a lopsided norm compatible with that of the characteristic region. Since this relies on very special structure in the field equations, the outlook for a complete proof of well posedness of CCM using existing Bondi-like gauges is, unfortunately, not rosy.

Our results signpost a number of paths to follow. First and foremost, we need to recover our numerical results for toy models for full GR. Beyond that, we seek a well-posed setup for the CIBVP that can be used in numerical applications with minimum change to existing code. For the latter, it will be useful to perform a pure gauge analysis along the lines of Refs. [58,59] to establish whether or not the blame for the degeneracy can be unambiguously laid on the coordinate choice, or if the specific construction of the formulations we discussed have some influence. Work in both directions is ongoing.

ACKNOWLEDGMENTS

We are grateful to Thomas Baumgarte, Nigel Bishop, Carsten Gundlach, Luis Lehner, and Denis Pollney for helpful discussions and/or comments on the manuscript. We also thank Mikel Sánchez for feedback on our Julia scripts. The work was partially supported by the FCT (Portugal) IF Programs No. IF/00577/2015, No. IF/00729/2015, and No. PTDC/MAT-APL/30043/2017 and Project No. UIDB/00099/2020. T. G. acknowledges financial support provided by FCT/Portugal Grant No. PD/BD/135425/2017 in the framework of the Doctoral Program IDPASC-Portugal. The authors acknowledge networking support by the GWverse COST Action CA16104, "Black holes, gravitational waves and fundamental physics."

[1] H. Bondi, M. G. J. van der Burg, and A. W. K. Metzner, Proc. R. Soc. A **269**, 21 (1962).
[2] R. K. Sachs, Proc. R. Soc. A **270**, 103 (1962).
[3] N. T. Bishop, R. Gómez, L. Lehner, M. Maharaj, and J. Winicour, Phys. Rev. D **56**, 6298 (1997).
[4] N. T. Bishop, R. Gómez, L. Lehner, and J. Winicour, Phys. Rev. D **56**, 6298 (1997).
[5] Y. Zlochower, R. Gómez, S. Husa, L. Lehner, and J. Winicour, Phys. Rev. D **68**, 084014 (2003).
[6] C. J. Handmer and B. Szilagyi, Classical Quantum Gravity **32**, 025008 (2015).
[7] K. Barkett, J. Moxon, M. A. Scheel, and B. Szilágyi, Phys. Rev. D **102**, 024004 (2020).
[8] J. Moxon, M. A. Scheel, and S. A. Teukolsky, Phys. Rev. D **102**, 044052 (2020).
[9] J. Winicour, Living Rev. Relativity **15**, 2 (2012).
[10] B. Szilágyi, Cauchy-characteristic matching in general relativity, Ph. D. thesis, University of Pittsburgh, 2000.
[11] P. M. Chesler and L. G. Yaffe, Phys. Rev. Lett. **106**, 021601 (2011).
[12] M. Attems, J. Casalderrey-Solana, D. Mateos, D. Santos-Oliván, C. F. Sopuerta, M. Triana, and M. Zilhão, J. High Energy Phys. 06 (2017) 154.
[13] B. Gustafsson, H.-O. Kreiss, and J. Oliger, *Time Dependent Problems and Difference Methods* (Wiley, New York, 1995).
[14] D. Hilditch, Int. J. Mod. Phys. A **28**, 1340015 (2013).
[15] M. C. Babiuc, S. Husa, D. Alic, I. Hinder, C. Lechner, E. Schnetter, B. Szilagyi, Y. Zlochower, N. Dorband, D. Pollney, and J. Winicour, Classical Quantum Gravity **25**, 125012 (2008).
[16] Apples with apples: Numerical relativity comparisons and tests.
[17] S. Frittelli and L. Lehner, Phys. Rev. D **59**, 084012 (1999).
[18] R. Gomez and S. Frittelli, Phys. Rev. D **68**, 084013 (2003).
[19] C. Gundlach and J. M. Martín-García, Classical Quantum Gravity **23**, S387 (2006).
[20] D. Hilditch and R. Richter, J. Hyper. Differ. Equations **12**, 1 (2015).
[21] T. Giannakopoulos, D. Hilditch, and M. Zilhão, Hyperbolicity of general relativity in bondi-like gauges, https://doi.org/10.5281/zenodo.3929666 (2020).
[22] S. Frittelli, Phys. Rev. D **71**, 024021 (2005).
[23] J. Winicour, Phys. Rev. D **87**, 124027 (2013).
[24] J. A. Crespo, H. P. de Oliveira, and J. Winicour, Phys. Rev. D **100**, 104017 (2019).
[25] P. M. Chesler and L. G. Yaffe, J. High Energy Phys. 07 (2014) 086.
[26] D. Hilditch, arXiv:1509.02071.
[27] A. Schoepe, D. Hilditch, and M. Bugner, Phys. Rev. D **97**, 123009 (2018).
[28] D. Hilditch and A. Schoepe, Phys. Rev. D **99**, 104034 (2019).
[29] H.-O. Kreiss and J. Lorenz, *Initial-Boundary Value Problems and the Navier-Stokes Equations* (Academic Press, New York, 1989).
[30] O. Sarbach and M. Tiglio, Living Rev. Relativity **15**, 9 (2012).
[31] N. T. Bishop, R. Gómez, P. R. Holvorcem, R. A. Matzner, P. Papadopoulos, and J. Winicour, Phys. Rev. Lett. **76**, 4303 (1996).
[32] N. T. Bishop, R. Gómez, P. R. Holvorcem, R. A. Matzner, P. Papadopoulos, and J. Winicour, J. Comput. Phys. **136**, 140 (1997).
[33] G. Calabrese, Classical Quantum Gravity **23**, 5439 (2006).
[34] C. W. Shu and S. J. Osher, J. Comput. Phys. **77**, 439 (1988).
[35] Jeff Bezanson, Alan Edelman, Stefan Karpinski, and Viral B. Shah, SIAM Rev. **59**, 65 (2017).
[36] C. Rackauckas and Q. Nie, J. Open Res. Software **5**, 15 (2017).
[37] M. Alcubierre *et al.*, Classical Quantum Gravity **21**, 589 (2004).
[38] G. Calabrese, I. Hinder, and S. Husa, J. Comput. Phys. **218**, 607 (2006).
[39] I. Hinder, Well-posed formulations and stable finite differencing schemes for numerical relativity, Ph.D. thesis, School of Mathematics, University of Southampton, 2005.
[40] M. Boyle, L. Lindblom, H. Pfeiffer, M. Scheel, and L. E. Kidder, Phys. Rev. D **75**, 024006 (2007).
[41] M. C. Babiuc *et al.*, Classical Quantum Gravity **25**, 125012 (2008).
[42] H. Witek, D. Hilditch, and U. Sperhake, Phys. Rev. D **83**, 104041 (2011).
[43] Z. Cao and D. Hilditch, Phys. Rev. D **85**, 124032 (2012).
[44] J. Thomas, *Numerical Partial Differential Equations: Finite Difference Methods*, Texts in Applied Mathematics (Springer, New York, 1998).
[45] A. Cabet, P. T. Chruściel, and R. T. Wafo, arXiv:1406.3009.
[46] D. Hilditch, J. A. V. Kroon, and P. Zhao, arXiv:1911.00047.
[47] D. Hilditch, J. A. V. Kroon, and P. Zhao, arXiv:2006.13757.
[48] J. M. Bardeen, O. Sarbach, and L. T. Buchman, Phys. Rev. D **83**, 104045 (2011).
[49] A. Zenginoglu, J. Comput. Phys. **230**, 2286 (2011).
[50] A. Vañó-Viñuales, S. Husa, and D. Hilditch, Classical Quantum Gravity **32**, 175010 (2015).
[51] A. Vañó-Viñuales, Free evolution of the hyperboloidal initial value problem in spherical symmetry, Ph.D. Thesis, University of Iles Balears, 2015.
[52] G. Doulis and J. Frauendiener, Phys. Rev. D **95**, 024035 (2017).
[53] D. Hilditch, E. Harms, M. Bugner, H. Rüter, and B. Brügmann, Classical Quantum Gravity **35**, 055003 (2018).
[54] A. Vañó-Viñuales and S. Husa, Classical Quantum Gravity **35**, 045014 (2018).
[55] E. Gasperin and D. Hilditch, Classical Quantum Gravity **36**, 195016 (2019).
[56] E. Gasperin, S. Gautam, D. Hilditch, and A. Vañó-Viñuales, Classical Quantum Gravity **37**, 035006 (2020).
[57] F. Beyer, J. Frauendiener, and J. Hennig, Int. J. Mod. Phys. D **29**, 2030007 (2020).
[58] A. M. Khokhlov and I. D. Novikov, Classical Quantum Gravity **19**, 827 (2002).
[59] D. Hilditch and R. Richter, Phys. Rev. D **94**, 044028 (2016).